硬岩の長期劣化予測を目的とした微視情報も算出可能な連続体理論の構築とその検証

課題番号：16560408

平成16年度から平成17年度科学研究補助金
（基盤研究(C)(2)）研究成果報告書

平成18年３月

研究代表者　奥井義昭
埼玉大学　工学部　助教授

はじめに

本報告書は科学研究費（基盤(c)）の補助を受けて行った平成16,17年度の研究成果をとりまとめたものである．竹村 貴人氏にについては科学研究費の申請時において埼玉大学に勤務していたが平成16年度に産業技術総合研究所へ異動したため，研究協力者として本研究に参加して頂きました．Dr. Golshani Aliakbar は埼玉大学理工学研究科博士課程を修了後，JSPS Postdocとして本研究に参加して頂きました．この場をかりて，謹んで謝意を表します．

研究組織

研究代表者：　奥井 義昭（埼玉大学工学部助教授）

研究分担者：　小田 匡寛（埼玉大学工学部　教授）

研究協力者：　竹村 貴人（産業技術総合研究所深部地質環境研究センター）

研究協力者：　Golshani Aliakbar（埼玉大学　JSPS Postdoc Researcher）

交付決定額（配分額）

（金額単位：円）

	直接経費	間接経費	合　計
平成16年度	2,900,000	0	2,900,000
平成17年度	900,000	0	900,000
総　　計	3,800,000	0	3,800,000

研究発表

- Golshani, A., Okui, Y., Oda, M., Takemura, T., "A micromechanical model for brittle failure of rock and its relation to crack growth observed in trixial compression tests of granite", Mechanics of Materials, 38, 2006, pp. 287-303.

- Golshani, A., Okui, Y., Oda, M., Takemura, T., "Hydraulic behaviour of Inada granite in the excavation disturbed zone around underground openings", The Seventh International Summer Symposium, JSCE, 30 July 2005 Tokyo, Japan, pp. 153-156.

- Golshani, A., Okui, Y., Oda, M., Suzuki, K., "Simulation of damage around a circular opening in rock". The 11th International Conference of IACMAG, 19-24 June, 2005, Turin, Italy, pp. 33-40.

- Golshani, A., Okui, Y., Takemura, T., Oda, M., "Time-dependent continuous damage model for brittle failure of rocks", 53rd Geomechanics Colloquy and EUROCK 2004, 7-9 October, 2004, Salzburg, Austria, pp.701-706.

ABSTRACT

The inelastic deformation of brittle materials such as crystalline rock occurs through growth of microcarcks under relatively low confining pressure. Microcracks propagate until failure, and the mechanical properties change considerably depending on the cracks concentration. Various continuum damage models have been proposed to describe mechanical behavior of brittle materials under compression. In spite of good prediction of rock strength, most of them do not have information on microcracks evolution which is very important for fluid flow through rock in various fields of engineering, such as nuclear waste isolation. The purpose of this study is to establish a micromechanics-based continuum damage model to analyze short and long-term behaviors of brittle rocks under compression. This model provides information on not only the macro-scale mechanical responses of rock such as strength, but also microcracks evolution with special emphasis on predicting numerically the changes in crack length and crack density during inelastic deformation. A small number of parameters are involved in this model and each one is physically meaningful and can be identified from the results of triaxial compression tests, creep tests and microscopic observation of microcracks.

This model is derived from the mechanics of tensile microcracks. It is assumed that local tensile stress which is generated as a result of sliding up on asperities, causes microcracks growth. Microcracks are tensile in nature and propagate in mode *I* (opening mode). The pre-existing microcracks may be randomly distributed or may have an initial preferential distribution. Also, they may be of varying sizes and orientations.

By generalizing the results obtained from the analysis of one single microcrack and also, including the effects of interaction among neighboring microcracks directly on cracks growth, a micromechanical continuum model for brittle rocks under compression is derived. Theory is formulated for an elastic solid containing microcracks. This procedure is based on the assumption that the matrix material remains elastic during loading and that all inelastic deformation is due to growth of microcracks.

In order to illustrate the predictive capability of the proposed model for mechanical properties of rock and cracks geometry evolution under compression (short-term behavior), the model is applied to Inada granite. Numerical results are compared with experimental data from triaxial compression tests results and microscopic observations of microcracks on Inada granite. The peak (failure) stress obtained numerically is in good accordance with the one observed in triaxial compression tests under a confining pressure higher than, say, 10 MPa. In the case of uniaxial tests in particular, the numerical model seriously overestimates the uniaxial strength. A major tension microcrack grows through the sample parallel to the axial direction in uniaxial tests, once the crack attains a critical length, while failure occurs in triaxial tests under confining pressures higher than 10 MPa only when the microcrack density is high enough. The overestimation probably reflects such a difference in the micromechanism leading to failure (peak stress). In spite of there difficulties, it can still be said that the proposed model has a chance of providing a sound basis for predicting crack growth, such as crack length and crack density, with sufficient accuracy. Also, it was found that only microcracks oriented in a cone of angle about 20 degree along the direction of greatest compressive stress propagate. Although, the microcracks in other directions do not grow, they affect the mechanical properties of rocks.

Furthermore, the present model is capable of reproducing the three characteristic stages of long-term (creep) behavior (i.e., primary, secondary and tertiary creep) commonly observed in laboratory creep tests. The sub-critical microcrack growth parameters (i.e. n and A) can be determined for Inada granite by fitting the numerical results of elapse time to failure versus the creep stress ratio curve with the experimental data under both dry and wet conditions. It is found that moisture has a significant influence on the parameter A rather than the parameter n. Use of the extended model makes it possible to analyze not only the extension of microcrack length, but also the development of the excavation damage zone (EDZ) around tunnels as a function of time. The disturbed zones mainly develop in the sidewalls of the tunnel in the case that the vertical stress σ_{22} is larger than the horizontal stress σ_{11}.

Table of Contents

Chapter 1: INTRODUCTION

1.1 Objectives 7

1.2 Study contents 7

Chapter 2: SHORT-TERM BEHAVIOR OF BRITTLE ROCK

2.1 Introduction 8

2.2 Microcrack damage model for brittle rocks 9

2.2.1 Microcrack growth model for a single microcrack 9

2.2.2 Interaction effect 14

2.2.3 Constitutive equation 17

2.3.4 Determination of length parameter d 20

2.3 Numerical simulation 21

2.3.1 Governing equations 22

2.3.2 Numerical analysis method 23

2.3.3 Simulation of two-dimensional biaxial compression test 26

2.3.3.1 Interaction effect 26

2.3.3.2 Effect of crack geometry 29

2.3.3.2.1 Crack density 29

2.3.3.2.2 Crack orientation 30

2.3.3.2.3 Initial crack length 32

2.4 Comparison of theory with experimental results 33

2.4.1 Inada granite 34

2.4.2 Model parameters 34

2.4.2.1 Elasticity parameters E and ν 34

2.4.2.2 Length parameter d and fracture toughness KIC 36

2.4.2.3 Density and length of microcracks 37

2.4.3 Numerical model 39

2.4.4 Strength of Inada granite 41

2.4.5 Microcrack growth 42

2.4.6 Crack density 44
2.4.7 Strength anisotropy 46
2.5 Conclusions 48
References 49

Chapter 3: LONG-TERM BEHAVIOR OF BRITTLE ROCK

3.1 Introduction 58
3.2 Governing equations 60
3.3 Numerical analysis method 61
3.4 Determination of parameters 62
3.5 Numerical simulation of biaxial tests 62
3.6 Long-term behavior in creep tests of Inada granite 65
3.6.1 Tests procedure 65
3.6.2 Experimental results 66
3.6.2.1 Creep tests on dry Inada granite 66
3.6.2.2 Effect of moisture 67
3.7 Long-term behavior of rock around a circular tunnel 69
3.8 Conclusions 73
References 74

Chapter 4: CONCLUSIONS AND FUTURE STUDIES

4.1 Conclusions 79
4.2 Future studies 80

Chapter 1

Introduction

Understanding the basic strength properties of rock has been a practical pursuit since ancient time, both because of the importance of mining and because rock was the principal building material. The crafting of stone tools required an intuitive grasp of crack propagation, and mining, quarrying, and sculpture are trades that require an intimate knowledge on the mechanical properties of rock. The design and excavation of quarries, for example, is a centuries-old art that relies on the recognition and exploitation of preferred splitting directions in order to maximize efficiency. One of the principal properties of brittle materials is that their strength in tension is much less than their strength in compression. This led, in architecture, to development of fully compressional structures through the use of arches and domes.

Rock was one of the first materials for which strength was studied with scientific scrutiny because of its early importance as an engineering material. By the end of nineteenth century the macroscopic phenomenology of rock fracture had been put on a scientific basis. The Mohr-Coulomb criterion had been developed and applied to rock fracture with sufficient success that it remains the principal tools used to describe this process for many engineering and geological applications.

All modern theories of strength recognize, either implicitly or explicitly, that real materials contain imperfections which produce the damage concentrations within the

body into a relatively small zone and result in rock fracture at much lower stresses than the theoretical strength.

Most rock materials posses an initial microcracks distribution related to their formation history and mineralogical composition. Behavior of microcracks impacts many branches of engineering including surface and underground mining, dam foundations, tunneling for hydro power and transport, petroleum reservoirs and nuclear waste storage. The use of underground storage in rock formation, for instance, makes the precise analysis of isolation properties of rock very important. The microcracks affect the isolation properties (permeability) of rocks around cavities and should be appropriately investigated and characterized.

Fracture of rock under multiaxial compression is often considered as a process in which increasing of load suddenly causes accelerated growth of the pre-existing cracks (short-term behavior). The following stages of brittle fracture of rock in multiaxial compression are revealed (Figure 1.1): 1) closing of pre-existing cracks (for uniaxial loading condition, in triaxial case the confining pressure closes the cracks before the deviatoric stress is applied), 2) loading without crack growth, 3) stable crack growth, and 4) unstable crack growth. Stable crack growth may, in principle, be controlled by the loading device, so that, for instance, a prescribed slow crack growth may be obtained. This is not possible for unstable crack growth, which occurs suddenly (Brace et al., 1966; Bieniawski, 1967; Broberg, 1973; Horii and Nemat-Nasser, 1985; Chudnovsky et al., 1988).

The onset of unstable crack growth occurs as a result of a global instability and leads to failure. The failure stress, usually referred to as the peak stress is followed by cracks coalescing and consequently rupture. In uniaxial compression, fracture results from unstable growth of a single crack while in triaxial compression, fracture occurs when the crack density increases over a threshold, which is global condition depending on all cracks (Hallbauer et al. 1973; Oda et al., 2002a). For a given confining pressure, a set of suitably oriented microcracks may suddenly become unstable under axial loading. The calculation of unstable crack growth requires numerical estimates which should include the interaction effects among microcracks. Indeed, without such interactions, no unstable crack growth would be predicted (Horii and Nemat-Nasser, 1983).

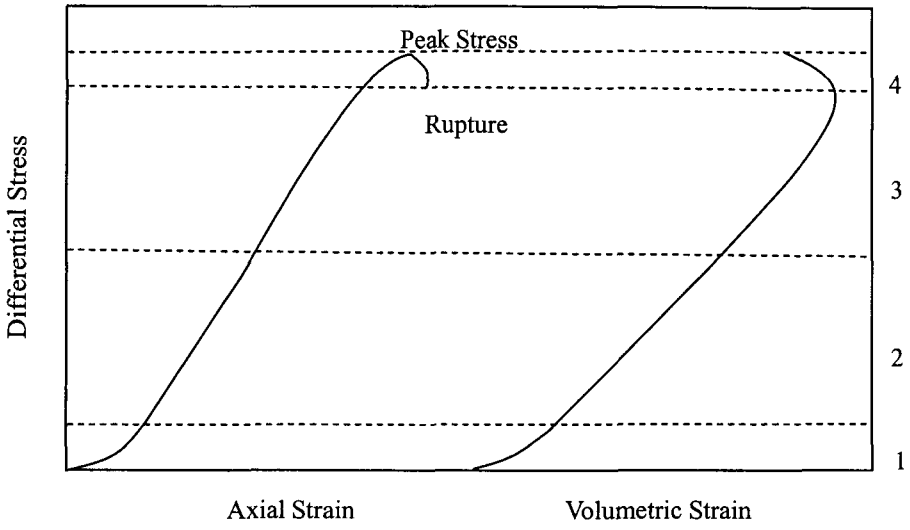

Figure 1.1 Mechanism of brittle fracture of rock in multiaxial compression.

On the other hand, long term behavior of brittle rocks under constant stress results form slow and stable growth of microcracks. Figure 1.2 shows a typical form of the relationship between strain and time during a creep test. This type of curve is called creep curve. The creep curve can be generally divided into three stages: 1) Primary creep 2) Secondary or steady creep and 3) Tertiary creep. The tertiary creep is the onset of macroscopic failure.

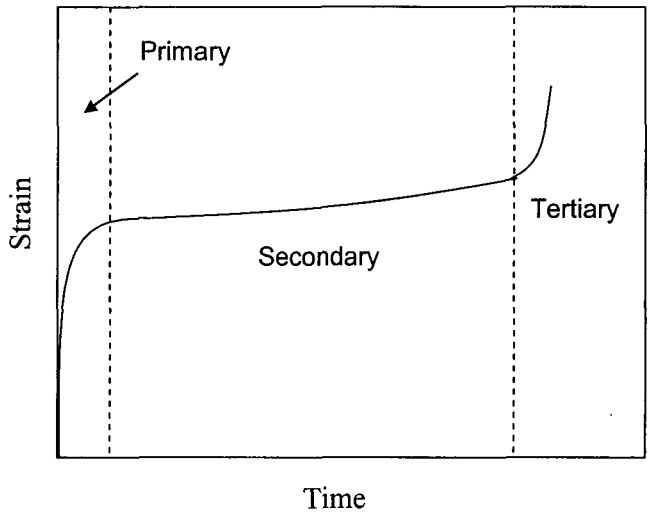

Figure 1.2 Relationship between strain and time during creep

In several materials with a highly heterogeneous structure such as rocks, microscopically small cracks may nucleate and pre-existing microcracks preferentially grow in size under axial compression with or without lateral confinement (Figure 1.3). These microcracks may eventually be linked together, causing macroscopic failure.

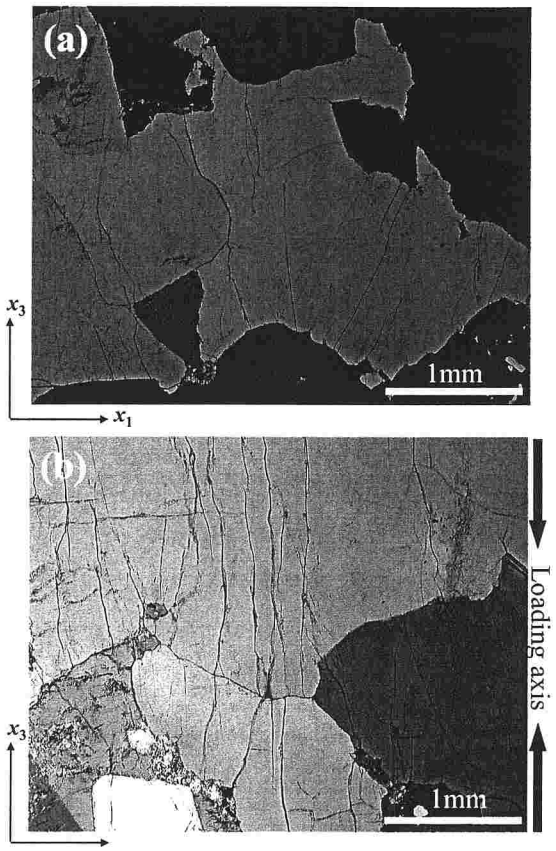

Figure 1.3 Photomicrograph of thin section, Inada granite; (a) Intact (b) Fractured (Takemura and Oda, 2002)

Through scanning electron microscope (SEM) and acoustic emission (AE) examinations, it is revealed that the onset and growth of microcracks dominate the failure and the macroscopic mechanical properties of rocks (Horii and Nemat-Nasser 1985, 1986; Wong 1985; Oda et al., 2002a, b).The main consequences can be summarized as follows: non linear stress-strain relationship, deterioration of elastic

properties, induced material anisotropy, significant volume dilatation, irreversible damage strains due to residual crack opening (Brace et al. 1966, Bieniawski 1967, Wawersik and Fairhurst 1970, Ofoegbu and Curran 1992). Although the complete process of progressive damage is quite complicated, it is still possible to quantify the degree of material damage, and to describe the progressive reduction of stiffness in term of some damage parameters.

It is important to understand the fracture mechanics of rock to improve its performance and to be able to predict its behavior. It should also be emphasized that fracture mechanics usually deals with the analysis of a single crack. However, in the deformation and failure of brittle rocks, one crack grows independent from other cracks only at relatively low stresses. Once numerous microcracks begin to grow, interaction among them starts to play a very important role in the evolution of further microcracking.

There are generally two families of continuum damage mechanics (CDM) theories to dealing with the non-elastic responses of brittle materials: the phenomenological approach and the micromechanical approach.

At first, phenomenological models with internal variable have been developed in the framework of thermodynamics of irreversible processes (e.g., Krajcinovic and Fonseka, 1981; Chow and Wang 1987a, b; Ju, 1989; Halm and Dragon 1996, 1998; Murakami and Kamiya, 1997; Swoboda and Yang, 1999a, b). The material damage is characterized by a set of scalar or tensorial internal variables, called damage parameters. The constitutive equations are derived from a postulated thermodynamic potential such as the Gibbs free energy function (e.g., Hayakawa and Kurakami, 1997). Such models provide macroscopic constitutive equations that can be easily applied to engineering analyses. However, the damage variables and thermodynamic potential are somewhat arbitrarily chosen based on mathematical conveniences rather than the physical interpretation of microcracking process (Shao et al., 1999; Shao and Rudnicki, 2000). For example, one class of phenomenological models is based on the concept of effective stress initially proposed by Kachanov (1958) for metal creep failure. Although the

physical meaning of this concept is clear in the isotropic case, the direct extension to the anisotropic case leads to nonsymmetric stress tensor. In addition, it remains unclear whether these models can accurately predict damage of brittle materials under compression stress. A variant of the phenomenological approach to develop CDM has been proposed by Ortiz (1985) and extended by Yazdani and Schreyer (1988). Their theory is based on the determination of a kinetic theory for damage induced strains. However, the material damage state is not properly defined by a physically based state variable.

In the micromechanical approach, on the other hand, the behavior of microcracks distributed in material is generally considered to explain the mechanical behavior of the material. Indeed, the growth of microcracks affects the effective elastic properties of the material. Various micromechanical models have been proposed (e.g., Costin 1983a, b, 1985; Nemat-Nasser and Obata 1988; Shi and Horii, 1989; Ju and Lee, 1990; Lee and Ju, 1990; Ju and Tseng, 1992; Okui et al., 1993; Prat and Bazant, 1996; Okui et al., 1997; Shao et al., 1999; Hoxha and Homand, 2000; Shao and Rudnicki, 2000). The sliding-crack model is often taken as a basis for the formulation of micromechanical models (Nemat-Nasser and Obata 1988; Kemeny and Cook, 1991). In other formulations the tensile cracks are also considered (Costin 1983a, b, 1985). The main advantage of micromechanical models is the ability to offer useful information on changes in density, length, aperture, and orientation of microcracks during inelastic deformation. This aspect is of great importance, particularly when we must consider coupling between induced inelastic strain and fluid flow through rock. Fluid no doubt flows through microcracks, which are produced as a result of damage growth. These models generally provide a clear physical meaning for their hypothesis and variables.

It should be noted here that, conventional micromechanical models were verified through comparison with only macroscopic experimental results, such as strengths and stress-strain relationships and the ability of the these models to reproduce the microstructure of actual rocks has not been investigated, even though recent microscopic observation techniques provide quantitative information on microscopic events in rock (e.g. Moore and Lockner, 1995; Takemura and Oda, 2003).

1.1 Objectives

The purpose of this study is to establish a micromechanics-based continuum damage model for brittle failure of rock under compression which describes evolution of microcracks as well as macroscopic stress-strain relationship for solid containing the microcracks, with paying considerable attention to the verification of the proposed model from a microscopic point of view.

This model can apply to a rock either contains randomly distributed microcracks or contains preferentially distributed microcracks. The microcarcks may be of varying sizes and orientations. Also, the effects of interaction among microcracks are directly taken into account in the proposed formulation (microcracks are dealt with together). For considering the interaction effects, the generalized form of Interaction Filed Theory IFT for microcracks with different orientation, is used. The proposed model contains a small number of parameters which can be determined easily from laboratory tests and each one is physically meaningful.

1.2 Study contents

The contents of this study are as follow:

In Chapter 2, the general concepts of the proposed theory are presented and the theory is formulated for rocks under compression stresses. Also, the model verification is performed through comparison of numerical results with experimental predictions and information on the microcracking of Inada granite.

The extended model for analyzing the long-term behavior of brittle rocks under compression comes in Chapter 3 and the developed model is applied to simulate the time-dependent development of EDZ around a circular tunnel in terms of the model parameters for Inada granite.

In Chapter 4, an overview of the main conclusions is presented along with the perspectives and recommendations for future extensions.

Chapter 2

Short-term Behavior of Brittle Rocks

2.1 INTRODUCTION

Brittle failure in rocks is the product of the nucleation and growth of microcarcks under relatively low confinement. While under high confining pressure, rocks exhibit ductile behavior. In the majority of the engineering problem, rocks behave as brittle materials and this study is limited to brittle behavior of rocks.

In section 2.2, the general concepts of the proposed model are presented and the theory is formulated for brittle failure of rocks under compression stresses. Also, the model parameters for the evolution law of microcracks are explained. Section 2.3 covers the numerical simulation of the proposed theory; governing equations, numerical analysis method and numerical results. In section 2.4, the proposed micromechanical theory verification is performed through comparison of numerical results with experimental predictions.

This model can apply to a rock either contains randomly distributed microcracks or contains preferentially distributed microcracks. The microcarcks may be of varying sizes and orientations. Also, the effects of interaction among microcracks are directly taken into account in the proposed formulation (microcracks are dealt with together). For considering the interaction effects, the generalized form of Interaction Filed Theory IFT for microcracks with different orientation (Okui et al., 1993), is used. The proposed model contains a small number of parameters which can be determined easily from laboratory tests and each one is physically meaningful.

2.2 MICROCRACK DAMAGE MODEL FOR BRITTLE ROCKS

In this section, a micromechanical model for microcrack growth based on mechanics of tensile microcracks is proposed. The interaction effect between microcracks are discussed by considering the boundary value problem of an elastic medium containing two microcracks (generalized form of interaction field theory IFT, Okui et al. 1993) and finally, the constitutive equation for the present model, is formulated through the homogenization of an elastic medium containing many microcracks with different orientations.

2.2.1 Microcrack growth model for a single microcrack

Mechanical behavior of brittle rocks under compression is known to be governed by growth of microcracks. To reproduce the behavior of rock under compressive stress, a microcrack growth model has been proposed. We can commonly detect three orthogonal planes called rift, grain and hardway in granitic rocks in the field. Interestingly, pre-existing microcracks are preferentially oriented parallel to the rift and grain planes, but much less to the hardway plane (e.g., Sano et al. 1992; Takemura et al., 2003). Analyzing the results of triaxial compression tests under confining pressures less than 140 MPa, Takemura (2002) has found that Inada and Ohshima granites fail in a two-dimensional fashion in the sense that microcracking (=crack growth) mainly occurs in a direction normal to the hardway plane. In other words, microcracks do not propagate equally, but rather the ones parallel to the rift and grain planes grow preferentially. This is the reason why microcracking was analyzed in a two-dimensional domain where global reference axes x_i $(i=1,2)$ are defined as shown in Fig. 2.1. The domain is small, but large enough in the sense that it consists of a large number of pre-existing microcracks. The domain, hereafter called the representative volume element (RVE), is subjected to far field stresses of σ_{11}, σ_{22} and σ_{12}.

Theoretical analyses suggest that so-called wing cracks propagate, like wings, from the two end tips of a pre-existing microcrack. In fact, wing cracks are well developed in laboratory tests using artificial cracks embedded in glass or plaster (e.g., Lajtai, 1971; Hoek and Bieniawski, 1984; Horii & Nemat-Nasser, 1986; Bobet & Einstein, 1998).

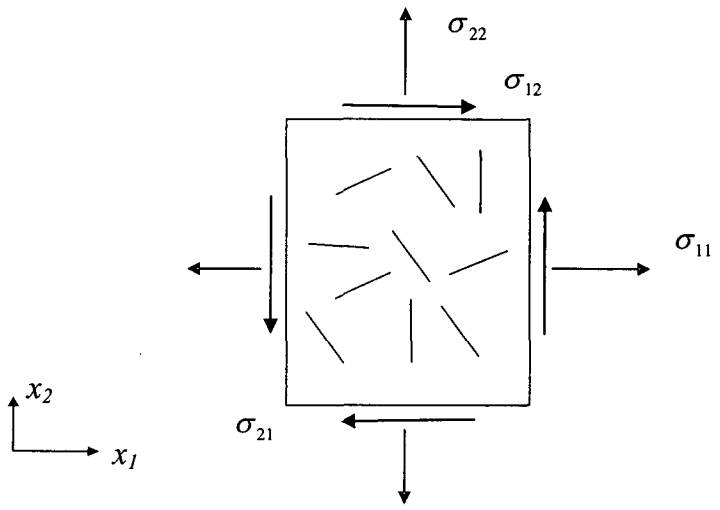

Figure2.1 Rock sample contains many microcracks with different orientations.

It is natural that damage growth was, until quite recently, commonly analyzed on the basis of the wing-crack model using a micro-mechanical approach (e.g., Horii & Nemat-Nasser, 1986; Okui, & Horii, 1997; Nemat-Nasser, & Obata, 1988; Li et al., 2000). However, it is suprising that development of wing cracks was seldom observed in actual triaxial compression tests on granitic rocks (e.g., Tapponnier & Brace, 1976; Wong, 1982; Oda et al., 2002). Instead, tension cracks in mode I commonly grow parallel to a major compression direction. The reason for this contradiction is not yet fully understood, but we should note a definite difference between actual and artificial cracks. Artificial cracks are flat, Griffith-like cracks, so that shear sliding may occur relatively easily on its contact surface. In the case of pre-exisitng microcracks in rock, on the other hand, they are seldom observed as flat surfaces, but rather appear to be undulating. As a result, each microcrack consists of a pair of undulating surfaces in contact with each other and even glued at some points.

What happens if such an undulating microcrack is subjected to differential stress? It seems reasonable to consider that shear sliding on the undulating surface remains rather small in the early stage of non-elastic deformation because of these asperities. As a

result, the surface can transmit shear stress much larger than that equal to the normal stress time frictional coefficient. In other words, the pre-existing microcrack is not really active in the early stage of deformation, but rather behaves like an elastic solid (matrix). This may also explain why wing cracks are seldom developed in actual rocks. That is, large shear sliding on a crack surface might be a necessary condition for developing such a wing crack.

Shear sliding must still occur on such an undulating surface, in particular in the later stage of deformation, although its magnitude remains relatively small. Importantly, the shear sliding always accompanies dilatational movement normal to the crack surface, so that the microcrack tends to open gradually. If this is the case, tensile stress might be generated at crack tips so that the pre-existing microcrack finally turns out to be an open microcrack. This idea is partially supported by the work of Horii and Nemat-Nasser (1985a, 1986). That is, the effect of sliding on a microcrack can be replaced in a mechanically equivalent manner by a pair of concentration forces acting normally to the crack surface.

In connection with this, Costin (1983a, b, 1985) has also postulated that local tensile regions, which give rise to crack growth, are generated around a microcrack, even when the stress is globally compressive. He did not fully discuss the mechanism leading to the local tensile stress, but only suggested that the heterogeneity of the rock may take part in the production of such local tensile regions.

Based on the above discussion, the microcrack surface is idealized as a smooth surface and the driving force is the local tensile stress σ_t' acting normal to the microcrack surface, which is generated as a result of sliding up on asperities. Referring to Costin's suggestion (Costin, 1983a, b, 1985; Rudnicki and Chau, 1996), we assume the following expression for σ_t' (Fig. 2.2):

$$\sigma_t = \sigma_{22}' + f(c)S_{22}' \tag{2.1}$$

The first term on the right hand side is due to the presence of a far filed compressive stress σ_{22}' perpendicular to microcrack which acts such as inhibit crack growth.

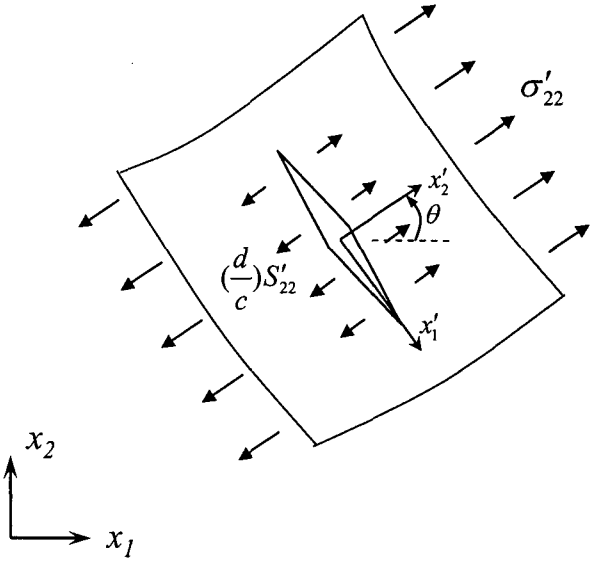

Figure 2.2 Idealized microcrack under local tensile stress

The second term is due to the effects of asperities which are assumed to be proportional to the component of the deviatoric stress S'_{22} $(=\sigma'_{22}-(\sigma'_{kk}/3)\delta_{ij})$ which is normal to microcrack surface. $f(c)$ is a proportionality coefficient depending only on c. In other words, the propagation condition is influenced by far field compression and controlled by deviatoric stress. It should be noted that the local tensile stress in Eq. (2.1) must decrease with increasing microcrack length $2c$. Otherwise, microcrack would propagate without limit. This unsatisfactory situation is easily avoided if the proportional coefficient $f(c)$ is inversely proportional to the half crack length c. Then we assume the following expression:

$$f(c)=\frac{d}{c} \tag{2.2}$$

here d stands for a typical scale of material such as grain size. Costin (1983a, b, 1985) has also introduced a length parameter similar to d, and interpreted it as the length of the local tensile stress region. In the present model however, we do not need such an explanation.

The x_i-axes are rigidly rotated to get local coordinate x_i'-axes. This rigid rotation can be expressed using an orthogonal tensor Ω_{ij} defined by

$$\Omega_{ij} = \cos(x_i' \wedge x_j) \quad (i = 1, 2 \text{ and } j = 1, 2) \tag{2.3}$$

where $(x_i' \wedge x_j)$ stands for the angle between the axes x_i' and x_j. Using Eq. (2.3), σ_{22}' and S_{22}' with respect to the local coordinate axes x_i' are written in term of the stresses with respect to the global coordinate axes x_i, as follows:

$$S_{22}' = \Omega_{2m}\Omega_{2n}S_{mn} = \Omega_{21}^2 S_{11} + \Omega_{22}^2 S_{22} + 2\Omega_{21}\Omega_{22}S_{12} \tag{2.4a}$$

$$\sigma_{22}' = \Omega_{2m}\Omega_{2n}\sigma_{mn} = \Omega_{21}^2 \sigma_{11} + \Omega_{22}^2 \sigma_{22} + 2\Omega_{21}\Omega_{22}\sigma_{12} \tag{2.4b}$$

and

$$\Omega_{21} = cos\theta \ , \ \Omega_{22} = \sin\theta$$

Therefore,

$$S_{22}' = S_{11}\cos^2\theta + S_{22}\sin^2\theta + S_{12}\sin 2\theta$$

$$= (\frac{\sigma_{11} - \sigma_{22}}{2})\cos^2\theta + (\frac{\sigma_{22} - \sigma_{11}}{2})\sin^2\theta + \sigma_{12}\sin 2\theta \Rightarrow$$

$$S_{22}' = (\frac{\sigma_{11} - \sigma_{22}}{2})\cos 2\theta + \sigma_{12}\sin 2\theta \tag{2.5a}$$

and

$$\sigma_{22}' = \cos^2\theta\ \sigma_{11} + \sin^2\theta\ \sigma_{22} + 2\sin\theta\ \cos\theta\ \sigma_{12} \tag{2.5b}$$

Using the local tensile stress of Eq. (2.1) we can calculate the stress intensity factor K_I of mode I as follows:

$$K_I = \sqrt{\pi\ c}[\sigma_{22}' + f(c)S_{22}'] \tag{2.6}$$

A criterion for the time-dependent crack growth law is now given in terms of a damage surface (i.e., $F = 0$) as follows:

$$F = K_I - K_{IC} = \sqrt{\pi\ c}[\sigma_{22}' + f(c)S_{22}'] - K_{IC} = 0 \tag{2.7}$$

where K_{IC} is the fracture toughness. Eq. (2.7) is called the microcrack growth law, through which the length $2c$ of the microcrack is controlled as a function of applied stresses.

Equation (2.7) is for a single crack in a given orientation. In order to move from the analysis of the behavior of individual cracks to a continuum theory, only one additional assumption is required. We assume that an ensemble of microcracks contained in some region of the body behaves in a manner similar to an individual crack. That is, the equation describing the response of an ensemble of cracks is identical in form to the equation which describes the response of a single isolated crack, Eq. (2.7), except that now c_i is the mean length of cracks with same orientation angle θ_i and, in the case of a system of many microcarcks, the interaction among microcracks should be considered.

2.2.2 Interaction effect

We have only considered growth of an individual microcrack in previous section independently of other microcracks, so that its use should be limited within the early stage of non-elastic deformation where interaction among microcracks is not dominant. To evaluate the elastic interaction among microcracks, the so-called pseudo-traction is used. This is a general, as well as powerful, method to solve problems which involve inhomogeneties such as microcracks in an elastic solid (Horii and Nemat-Nasser, 1985a, b). To outline the principle, we first consider an infinite plane with two microcracks α and β of lengths $2c_\alpha$ and $2c_\beta$, respectively, which is subjected to the far filed stresses. Two coordinate systems: $x_i'^{\alpha}$ and $x_i'^{\beta}$ (i=1, 2) are employed such that their origins: O_α and O_β, are located at the centers of the microcracks α and β. Note that the $x_2'^{\alpha}$ and $x_2'^{\beta}$ are taken to be normal to the microcrack surfaces. The distance between origins of microcracks is $d_{\alpha\beta}$. The original problem is decomposed into a homogenous problem and two subproblems as shown in Figure 2.3.

The symbols in Fig. 2.4 are defined as

$d_{\alpha\beta}$ = the distance between origins of microcracks α and β.

$\theta_{\beta\alpha}$ = the inclination angle of $x_2'^{\alpha}$ to $x_2'^{\beta}$.

$\phi_{\beta\alpha}$ = the angle between $x_1'^{\alpha}$ and $O_\alpha O_\beta$ direction.

The original boundary problem is decomposed into three sub-problems; i.e., one homogenous sub-problem and two sub-problmes α and β (Fig. 2.4).In the homogenous problem, there is no microcrack and the same far field stresses as the original problem are applied. In.subproblem α, for example, one microcrack α is considered in the infinite solid under zero stresses at infinity.

The stress free condition on surfaces of microcrack α in the original problem is satisfied as follows:

$$\sigma'_{22}+\sigma'^{\alpha}_{22}+\sigma'^{P\alpha}_{22}=0\Rightarrow\sigma'_{22}=-(\sigma'^{\alpha}_{22}+\sigma'^{P\alpha}_{22}) \tag{2.8}$$

$$\sigma'_{12}+\sigma'^{\alpha}_{12}+\sigma'^{P\alpha}_{12}=0\Rightarrow\sigma'_{12}=-(\sigma'^{\alpha}_{12}+\sigma'^{P\alpha}_{12}) \tag{2.9}$$

where σ'_{22} and σ'_{12} are the stresses on the surface of microcrack α in subproblem α, with respect to local coordinate x'^{α}_{i} (i=1, 2). σ'^{α}_{22} and σ'^{α}_{12} denote the stresses in the homogenous problem at the position of microcrack α, and the quantities $\sigma'^{P\alpha}_{22}$ and $\sigma'^{P\alpha}_{12}$, which called pseudo-tractions, are the stresses at the position of the microcrack α in subproblem β (caused by microcrack β).

The pseudo-tractions must be determined such that all the boundary conditions for the original problem are satisfied. Using Muskhelishivili complex stress function, consistency equation which ensures the traction-free condition of the surface of microcrack, can be expressed as following expression with respect to local coordinate (see Okui et al., 1993):

$$\{\sigma'^{P\alpha}\}=[\gamma'^{\alpha\beta}](\{\sigma'^{\beta}\}+\{\sigma'^{P\beta}\}) \tag{2.10}$$

where

$$\sigma'^{P\alpha}=\{\sigma'^{P\alpha}_{11},\sigma'^{P\alpha}_{22},\sigma'^{P\alpha}_{12}\}^{T},\sigma'^{\beta}=\{\sigma'^{\beta}_{11},\sigma'^{\beta}_{22},\sigma'^{\beta}_{12}\}^{T}$$

and

$$[\gamma'^{\alpha\beta}]=\frac{1}{2}\left(\frac{c_\beta}{d_{\alpha\beta}}\right)^{2}\begin{bmatrix} a_1[1+\frac{1}{2}(\frac{d}{c_\beta})] & a_1[-\frac{1}{2}(\frac{d}{c_\beta})] & a_4 \\ a_2[1+\frac{1}{2}(\frac{d}{c_\beta})] & a_2[-\frac{1}{2}(\frac{d}{c_\beta})] & a_5 \\ a_3[1+\frac{1}{2}(\frac{d}{c_\beta})] & a_3[-\frac{1}{2}(\frac{d}{c_\beta})] & a_6 \end{bmatrix} \tag{2.11}$$

where σ'^{β} is the stress at the position of the microcrack β arising from far field stress in the homogenous sub-problem, and the additional parameters $a_i (i = 1,2,...,6)$ are given in terms of the geometrical quantities in Fig. 2.3, as follows:

$a_1 = \cos 2\phi_{\alpha\beta} - \cos 2(2\phi_{\alpha\beta} - \theta_{\alpha\beta}) + \cos 2(\phi_{\alpha\beta} - \theta_{\alpha\beta})$,

$a_2 = \cos 2\phi_{\alpha\beta} + \cos 2(2\phi_{\alpha\beta} - \theta_{\alpha\beta}) - \cos 2(\phi_{\alpha\beta} - \theta_{\alpha\beta})$,

$a_3 = \sin 2(\phi_{\alpha\beta} - \theta_{\alpha\beta}) - \sin 2(2\phi_{\alpha\beta} - \theta_{\alpha\beta})$,

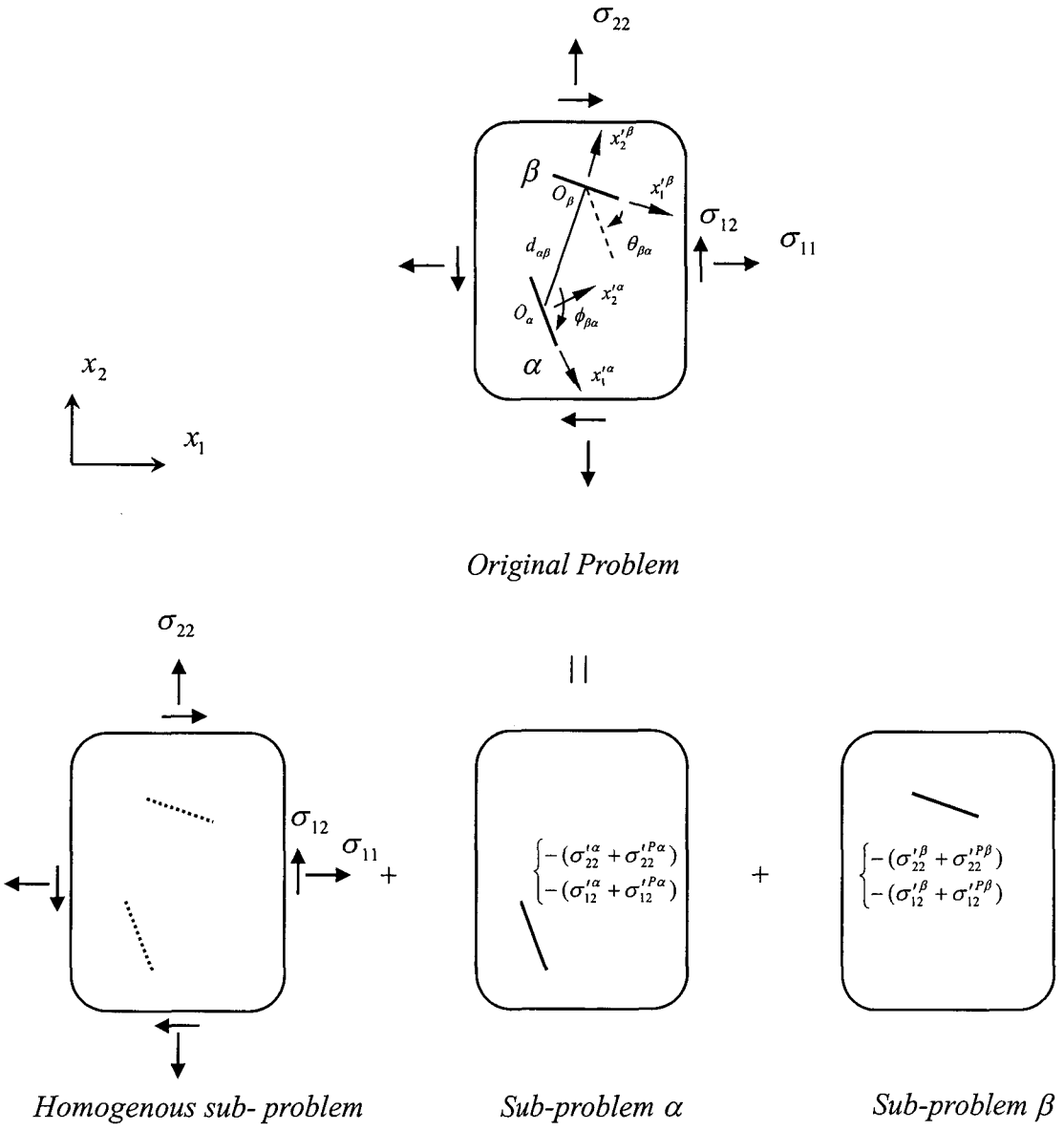

Figure 2.3 Decomposition of an original problem

$$a_4 = \sin 2\phi_{\alpha\beta} - \sin 2(2\phi_{\alpha\beta} - \theta_{\alpha\beta}),$$
$$a_5 = \sin 2\phi_{\alpha\beta} + \sin 2(2\phi_{\alpha\beta} - \theta_{\alpha\beta}),$$
$$a_6 = \cos 2(2\phi_{\alpha\beta} - \theta_{\alpha\beta})$$

We considered only two microcracks in Eq. (2.10). In reality, however, a huge number of microcracks are distributed in the domain. When all the sub-problems are taken into account, the consistency equation (2.10) can be generalized as an integral equation for microcracks.

Considering the effects of the interaction, we can easily rewrite the damage laws of Eq. (2.7) as

$$F(\sigma', \sigma'^{P}, c) = \sqrt{\pi\, c}\left[(\sigma'_{22} + \sigma'^{P}_{22}) + f(c)\left(\frac{(\sigma'_{22} + \sigma'^{P}_{22}) - (\sigma'_{11} + \sigma'^{P}_{11})}{2}\right)\right] - K_{IC} \qquad (2.12)$$

2.2.3 Constitutive equation

To formulate constitutive equations, rock is idealized as an elastic solid with many microcracks distributed at different orientations (Figure 2.1). Analysis is done based on the assumption that the rock element remains elastic during loading and that all inelastic deformation is due to microcrack growth (brittle behavior). All microcracks are classified into *N*-groups, depending on their orientations. It is assumed, just for simplicity, that all microcracks belonging to *i*th group have the same length $2c_0^{(i)}$ and the same orientation $\theta^{(i)}$. Here, $\theta^{(i)}$ is defined as the inclination angle of a unit vector normal to the crack surface of the global axis x_1.

First, we consider the total strain $\varepsilon_t'^{(i)}$ associated with the simplest case that one microcrack, belonging to an *i*th group exist in an elastic solid, which is subjected to far field stress σ'_{ij}. The total strain can be decomposed into two parts: an elastic strain due to the elastic deformation of matrix ($\varepsilon_e'^{(i)}$) plus the inelastic strain associated with the opening of the microcrack ($\hat{\varepsilon}'^{(i)}$) (Note that all the strains and stresses are defined with respect to the local axes $x'_i (i = 1,2)$):

$$\varepsilon_t'^{(i)} = \varepsilon_e'^{(i)} + \hat{\varepsilon}'^{(i)} \qquad (2.13)$$

Let $[u_2']^{(i)}$ be the opening displacement jump equal to $\left(u_2'^{+} - u_2'^{-}\right)^{(i)}$ where $\left(u_2'^{+}\right)^{(i)}$ and $\left(u_2'^{-}\right)^{(i)}$ are the displacements taking place while opening from 0 to on the positive and negative sides of the microcrack, respectively. Using the local axes $x_i'(i=1,2)$, we obtain the following expression (Nemat-Nasser and Horii, 1993):

$$[u_2']^{(i)} = \frac{\kappa+1}{2G}\sqrt{\left(c^{(i)}\right)^2 - x_1'^2}\,\sigma_t' \tag{2.14}$$

where G is the shear modulus of matrix material, κ is Lame parameter:

$$\kappa = \begin{cases} 3-4\nu & plane\ \ strain \\ \dfrac{3-\nu}{1+\nu} & plane\ \ stress \end{cases} \tag{2.15}$$

Of course, Eq. (2.14) is valid only when $|x_1'| \le c^{(i)}$. It should be noted that the sliding displacement jump $[u_1']^{(i)}$ parallel to the crack surface is neglected since it is considered, as dicussed in the previous section, that its effect on the inelastic strain is small compared with that of $[u_2']^{(i)}$. The average inelastic strain induced by the opening displacement jump is obtained as

$$\hat{\varepsilon}'^{(i)} = \frac{1}{2V_e}\int_{-c}^{c}\left(\boldsymbol{n}'^{(i)} \otimes [\boldsymbol{u}']^{(i)} + [\boldsymbol{u}']^{(i)} \otimes \boldsymbol{n}'^{(i)}\right)dx_1' \tag{2.16}$$

where $\boldsymbol{n}'^{(i)}$ is the unit vector normal to the microcrack surface and $\left[\boldsymbol{n}'^{(i)}\right] = \begin{Bmatrix} 0 & [u_2']^{(i)} \end{Bmatrix}^T$. Since $\boldsymbol{n}'^{(i)}$ is parallel to the local axis x_2', then we have $\boldsymbol{n}'^{(i)} = \begin{Bmatrix} 0 & 1 \end{Bmatrix}^T$. Let $m^{(i)}$ be the total number of microcracks belonging to the ith group. Integrating Eq. (2.16), we have a non-zero component of $\hat{\varepsilon}'^{(i)}\left(=(m^{(i)}/V_c)\int_{-c}^{c}[u_2']^{(i)}dx_1'\right)$. Thus, we have:

$$\hat{\varepsilon}'^{(i)} = \frac{\rho^{(i)}\pi(c^{(i)})^2(\kappa+1)}{4G}\begin{pmatrix} 0 \\ \sigma_{22}' + \left(\dfrac{d}{c^{(i)}}\right)S_{22}' \\ 0 \end{pmatrix} \tag{2.17}$$

where $\rho^{(i)}\left(=m^{(i)}/V_e\right)$ is the number density of microcracks belonging to the ith

group. Since the inelastic strain tensor of Eq. (2.17) is calculated using the local reference axes, we must rotate the local axes by $(\pi/2-\theta^{(i)})$ to obtain the corresponding strain tensor $\hat{\varepsilon}^{(i)}$ in the global coordinate axes $x_i (i=1,2)$. The result is written as

$$\{\hat{\varepsilon}\}^{(i)} = [C]^{(i)} \{\sigma\} \tag{2.18}$$

Summing up Eq. (2.18) over N groups, we finally have the following expression for the inelastic strain $\hat{\varepsilon}$ arising from all microcracks.

$$\{\hat{\varepsilon}\} = \sum_{i=1}^{N} \{\hat{\varepsilon}\}^{(i)} = \sum_{i=1}^{N} [C]^{(i)} \{\sigma\} = [C]\{\sigma\} \tag{2.19}$$

(or $\hat{\varepsilon} = C : \sigma$)

where

$$[C]^{(i)} = \frac{\rho^{(i)} \pi (c^{(i)})^2 (1+\kappa)}{8G} \times$$

$$\begin{bmatrix} 2\cos^4\theta^{(i)} + b_1(\frac{d}{c^{(i)}}) & 2\cos^2\theta^{(i)}\sin^2\theta^{(i)} - b_1(\frac{d}{c^{(i)}}) & 2\cos^2\theta^{(i)}\sin 2\theta^{(i)}[1+(\frac{d}{c^{(i)}})] \\ 2\sin^2\theta^{(i)}\cos^2\theta^{(i)} + b_2(\frac{d}{c^{(i)}}) & 2\sin^4\theta^{(i)} - b_2(\frac{d}{c^{(i)}}) & 2\sin^2\theta^{(i)}\sin 2\theta^{(i)}[1+(\frac{d}{c^{(i)}})] \\ 2\sin\theta^{(i)}\cos^3\theta^{(i)} + b_3(\frac{d}{c^{(i)}}) & 2\sin^3\theta^{(i)}\cos\theta^{(i)} - b_3(\frac{d}{c^{(i)}}) & \sin^2 2\theta^{(i)}[1+(\frac{d}{c^{(i)}})] \end{bmatrix}$$

(2.20)

and

$$\begin{aligned} b_1 &= \cos 2\theta^{(i)} \cos^2\theta^{(i)} \\ b_2 &= \cos 2\theta^{(i)} \sin^2\theta^{(i)} \\ b_3 &= 0.5 \sin 2\theta^{(i)} \cos 2\theta^{(i)} \end{aligned} \tag{2.21}$$

In case of one set crack with $\theta = 0$ and length of $2c$:

$$b_1 = 1, \quad b_2, b_3 = 0 \Rightarrow \text{ Vertical cracks } \& \quad [C] = \frac{\rho\pi\, c^2 (1+\kappa)}{8G} \begin{bmatrix} 2+(\frac{d}{c}) & -(\frac{d}{c}) & 0 \\ 0 & 0 & 0 \\ 0 & 0 & 0 \end{bmatrix}$$

The stress-strain relationship for an elastic material containing many microcracks is given by (e.g., Horii and Nemat-Nasser, 1983)

$$\sigma = D_e : \varepsilon_e \tag{2.22}$$

or

$$\sigma = D_e : (\varepsilon_t - \hat{\varepsilon}) \tag{2.23}$$

where D_e is the elastic modulus tensor for the matrix and the symbol (:) stands for the inner product. Assuming that the matrix is elastically isotropic, it is given in terms of Young's modulus E and Poisson's ratio ν. For a plane strain case, for example, we have

$$D_e = \frac{E}{(1+\nu)(1-2\nu)} \begin{bmatrix} 1-\nu & \nu & 0 \\ \nu & 1-\nu & 0 \\ 0 & 0 & (1-2\nu)/2 \end{bmatrix} \tag{2.24}$$

For a plane stress case, we also have

$$D_e = \frac{E}{(1-\nu^2)} \begin{bmatrix} 1 & \nu & 0 \\ \nu & 1 & 0 \\ 0 & 0 & (1-\nu)/2 \end{bmatrix} \tag{2.25}$$

Using Eq. (2.19) in Eq. (2.23), we finally have the stress-strain relationship, as follows:

$$\varepsilon = D_e^{-1} : (I + D_e : C) : \sigma \tag{2.26}$$

2.2.4 Determination of length parameter *d*

Parameter d in Eq. (2.2) was introduced as a typical size for related material. It seems reasonable to consider that the length d might be related to the grain size. Similarly, the half-length c_0 of microcracks also increases with increasing grain size (Peng and Johnson, 1972; Sprunt and Brace, 1974; Hadley, 1976; Chen et al., 1979; Wong et al, 1996). Accordingly, it can be assumed that the ratio d/c_0 is constant,

being independent of the grain size.

The present model tells us that under triaxial test condition, microcracks parallel to maximum principal compressive stress (i.e., $\theta = 0$) grow first. Furthermore, it can be said that microcracks may grow independently at the initial microcracking stage. If this is the case, the effect of elastic interaction can be neglected so that the microcrack growth law of Eq. (2.7) is applicable for detecting a stress point, at beyond $2c_0$. Substituting $\sigma'_{22} = \sigma_{11}$ (=confining pressure), $\sigma'_{11} = \sigma_{22}$ (=axial stress) and $c = c_0$ in Eq. (2.7) and rearranging these terms, we obtain the following expression for representing an initial damage surface:

$$S_{11} + \frac{1}{(\frac{d}{c_o})}\sigma_{11} - \frac{K_{IC}}{\sqrt{\pi\, c_o}(\frac{d}{c_o})} = 0 \tag{2.27}$$

Now the constant $(d/c_0)^{-1}$ can be determined from the slope in the relationship between the deviatoric stresses S_{11} at an initial damage point C' and the applied confining pressures σ_{11} (Fig. 2.4).

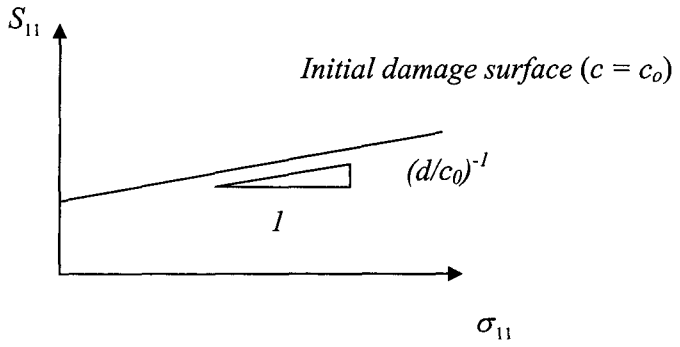

Figure 2.4 Deviatoric stress at the initial damage versus confining pressure

2.3 NUMERICAL SIMULATION

The governing equations for the microcrack damage model are formulated through the homogenization of an elastic solid with many microcracks of different orientation in

this section. Then, the numerical analysis method, Finite Element Method (FEM) which is used for simulation of the proposed model is explained, briefly. Finally, this simulation is applied to a simple example (biaxial compression test) and the effects of model parameters, microcracks geometry and interaction effect among microcracks on mechanical properties of rocks are discussed.

2.3.1 Governing equations

In this section, the formulation for the discrete system shown in section two is generalized for a continuous medium which contains many distributed microcracks using homogenization and the interaction effect among microcracks also, is considered. Note that by considering interaction effect directly in governing equations, microcracks are dealt with together. The stress and strain tensors σ and ε and the displacement vector u are the averaged quantities over a representative volume element. The governing equations are as follow as

I) Equilibrium equation

$$\nabla \cdot \sigma + b = 0 \tag{2.28}$$

where b is the body force, $(\nabla)_i = \partial / \partial x_i$ and "." is scalar product.

II) Strain-displacement relationship

$$\varepsilon = \frac{1}{2}(\nabla \otimes u + (\nabla \otimes u)^T) \tag{2.29}$$

where "$\otimes$" denotes tensor product.

III) Stress-strain relationship

$$\sigma = D_e : (I - H) : \varepsilon \tag{2.30}$$

where

$$H = (I + C : D_e)^{-1} : C : D_e \tag{2.31}$$

and $\boldsymbol{I}$ and D_e are the identity and elastic modulus tensors, respectively.

IV) Evolution equation

$$\begin{cases} F = 0 & \text{(possible growth)} \\ F < 0 & \text{(no growth)} \end{cases} \tag{2.32}$$

Considering interaction effect among microcracks, the damage law with respect to the global coordinate axes $x_i (i = 1,2)$ is rewritten as

$$F(\sigma,\sigma^P,c) = \sqrt{\pi\, c}\left[(\sigma_{11} + \sigma_{11}^P) + f(c)\left(\frac{(\sigma_{11} + \sigma_{11}^P) - (\sigma_{22} + \sigma_{22}^P)}{2}\right)\right] - K_{IC} \tag{2.33}$$

V) Consistency equation

Since many microcracks are considered and the number of the sub-problems is infinite, the consistency condition, which ensures the traction-free condition of the surface, can be generalized as an integral equation (Okui et al., 1993). Consider N groups of microcracks, we can rewrite Eq. (2.10) with respect to the global axes $x_i (i = 1,2)$, as follows:

$$\sigma^P(x) = \sum_{i=1}^{N} \rho^{(i)} \int_v \gamma(x/\xi)\{\sigma(\xi) + \sigma^P(\xi)\} d\xi \tag{2.34}$$

where $\gamma(x/\xi)$ is the same definition of $\gamma_{ij}^{\prime\alpha\beta}$ as in Eq. (2.11), except $d_{\alpha\beta} = |x - \xi|$ and c_β and $\phi_{\alpha\beta}$ are replaced by the half crack length at the point ξ: $c(\xi)$ and $\phi = \tan^{-1}[(x_2 - \xi_2)/(x_1 - \xi_1)] + \pi/2$, respectively.

2.3.2 Numerical Analysis method

The finite element method is used to perform the numerical calculation for governing equations of the proposed model. The first step in the finite element method is descretization. In this simulation, the displacement is approximated to be linear in a three nodes triangular element. At any point inside of an element, the displacement is expressed in terms of nodal displacements; this is done by writing the displacements as a linear combination of shape functions. There is one shape function for each of the three nodes of a triangular element. A shape function associated with a particular node

varies linearly from unity at that node to zero at the remaining nodes. The microcrack length and the interaction tensor are also approximated to be constant.

By discretization, $2N^p$ equilibrium equations are obtained, in which N^p is the total number of nodal points. Also, the evolution law $F = 0$ is descretized to $N \times N^e$ algebraic equations where N^e and N are the total number of elements and number of microcracks groups, respectively. By evaluating the integral in equation (2.34) numerically, the consistency equation is reduced to $3N^e$ nonlinear algebraic equations. Thus, we have a system of $2N^p + (N+3)N^e$ nonlinear equations and $2N^p + (N+3)N^e$ unknowns. The unknowns are the $2N^p$ nodal displacements, $N \times N^e$ microcracks length (for N groups of microcracks) and $3N^e$ element interaction field.

We have as a result, the following system of nonlinear algebraic equations for the discretized displacement $\bar{u}$, the interaction tensor $\bar{\sigma}^P$ and the microcracks length $\bar{c}$ in vector form:

1) $K\bar{u} - \bar{q} = 0$; $2N^p$ equilibrium equations (2.35)

where K is stiffness matrix $(2N^e \times 2N^e)$, and $\bar{q}$ is body force vector $(1 \times 2N^e)$.

2) $(\mathrm{I} - \Gamma)\bar{\sigma}^P - \Lambda\bar{u} = 0$; $3N^e$ consistency equations (2.36)

I is identity matrix $(3N^e \times 3N^e)$ and Γ and Λ are defined as follows:

$$\Gamma = \sum_{i,j}^{N^e,N^e} \bar{\gamma}^{ij} = \sum_{i,j}^{N^e,N^e} \sum_{k=1}^{N} \int_{V_j} \rho^{(k)} \gamma(\bar{x}^i / \xi) d\xi \tag{2.37}$$

$$\Lambda = \sum_{i,j}^{M,M} \bar{\gamma}^{ij} S^j \tag{2.38}$$

V_j and $\bar{x}^i$ denote the area of element j and the centroid of element i, respectively; S^j is the stress matrix of element j (Figure 3.1). Note that K, Γ and Λ are nonlinear functions of $\bar{c}$, θ (inclination angle of $n^{(k)}$ unit vector normal to the kth group of microcracks

to the far field confining pressure axis) and $\rho^{(k)}$ (density of kth group of microcracks).

3) $f(\bar{u},\bar{c},\bar{\sigma}^P)=0$; $N\times N^e$ evolution equations (2.39)

The Newton-Raphson method is used to solve the system of $2N^p+(N+3)N^e$ nonlinear equations. This method is very popular also in the multidimensional case as well as in the one-dimensional case; it is very efficient if there is a good initial approximation. For simplicity the system of the nonlinear equations is expressed as

$$F(\zeta,\chi)=0 \tag{2.40}$$

where ζ and χ are the control and unknown vectors, respectively. If load vector method is used, these vectors are assigned to $\bar{q}$ and $\{\bar{u}\ \ \bar{c}\ \ \bar{\sigma}^P\}$, respectively. Using the initial values $(\zeta_0\ \ \chi_0)$, under the given increment of control vector $\Delta\zeta$, we seek the increment $\Delta\chi$ which satisfies

$$F(\zeta_0+\Delta\zeta,\chi_0+\Delta\chi)=0 \tag{2.41}$$

In neighborhood of χ_0, equation (2.41) can be expanded in Taylor series and by neglecting terms of second order and higher, we have

$$J.\delta\chi\ =-F(\zeta_0+\Delta\zeta_0,\chi_0) \tag{2.42}$$

where J is the Jacobian matrix as follows:

$$J(\zeta,\chi)=\left[\frac{\partial F}{\partial\chi}\right](\zeta,\chi) \tag{2.43}$$

After solving matrix equation (2.43), corrections are added to the initial values of unknown vectors. The process is iterated to convergence and

$$\Delta\chi=\sum_{k=1}^{i}\delta\chi^k \tag{2.44}$$

where i is the iteration counter.

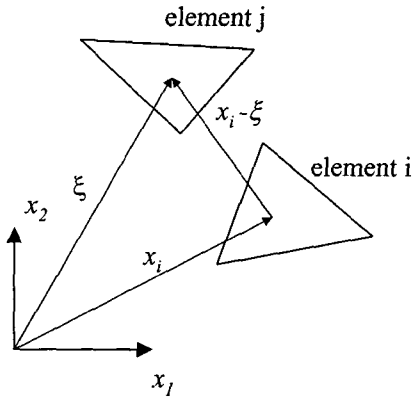

Figure 2.5 Elements i and j

2.3.3 Simulation of two-dimensional biaxial compression test

In this section, a simple numerical example is proposed and the effect of the model parameters on mechanical properties of rocks will be discussed. We consider a biaxial compression test of a rock sample (Figure 2.6). The dimensions of the sample are $200c_r \times 200c_r$, where $c_r = 1.00mm$ (half of the reference cracks length). Both top and bottom boundaries of the rock sample are assumed to be smooth. The model parameters are assumed as follows: $K_{IC} = 2.5\ MPa\ m^{1/2}$, Poison's ration $\nu = 0.23$ and normalized Young's modulus $E/\sigma_r = 1150$. It should be noted that, for normalizing stresses values, the reference stress σ_r is used and it is defined by $\sigma_r = K_{IC}/\sqrt{\pi\ c_r}$ with the fracture toughness of the material K_{IC}. First, sample is subjected to hydrostatic stress by applying a uniform pressure at the lateral boundaries in combination with enough axial displacement (Δ) to achieve an isotropic inplane stress state. After the hydrostatic load reaches a specific normalized confining compression σ_{11}/σ_r, only axial displacement increases until the rock material failure. During this loading, the lateral pressure is kept constant.

2.3.3.1 Interaction effect

For investigating the interaction effect, it is assumed that the rock sample contains one group of microcarcks (vertical) with normalized cracks density of $\rho\ c_r^2 = 0.12$. Other parameters are assumed as follows; length parameter $d = 0.69c_0$ and initial microcracks length $2c_0 = 1.00\ mm$. Figure 2.7 shows the microcracks growth in elements 1-4 with the normalized confining pressure $\sigma_{11}/\sigma_r = 0.80$ (compression is

positive) for with and without interaction effect cases.

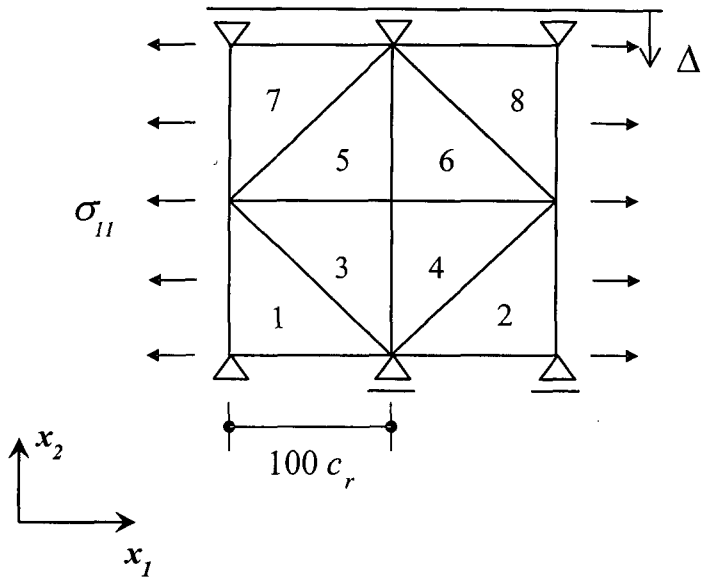

Figure 2.6 Finite element mesh of a biaxial test

At the initial loading stage, microcracks growth for both cases is identical. The growth of microcracks in case of considering interaction effect is more accelerated with increasing axial load due to interaction among microcracks. Furthermore, the damage distribution gradually loses its uniformity in the specimen depend on interaction stress with axial loading increment. However, the damage distribution is identical for all elements and there is no peak axial stress point for the case without interaction effect. Also, relationship between normalized differential stress and volumetric strain (Figure 2.8) show the same results.

In Figure 2.9, relationship between normalized axial stress and normalized interaction stress for two elements are shown. Interaction stress increment accelerates gradually with axial loading increasing and consequently leads to acceleration of microcracks growth. Also it is not identical in different elements.

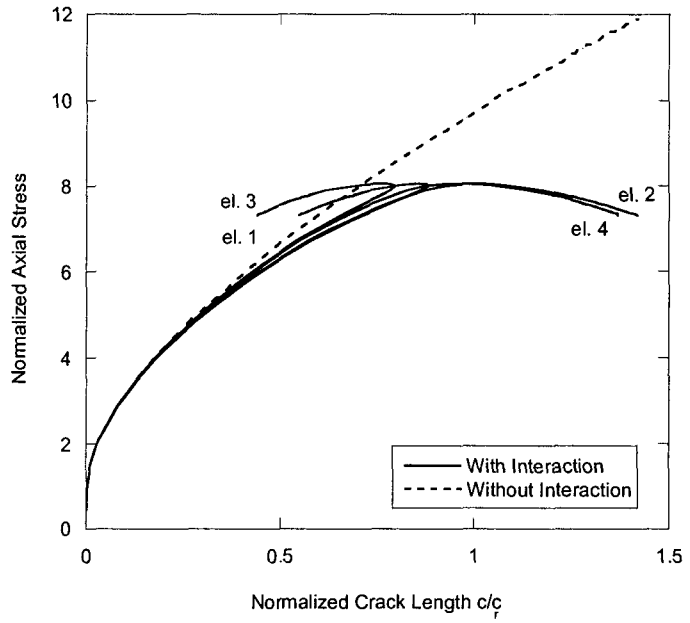

Figure 2.7 Normalized axial stress versus normalized cracks length for $\sigma_{11}/\sigma_r = 0.80$.

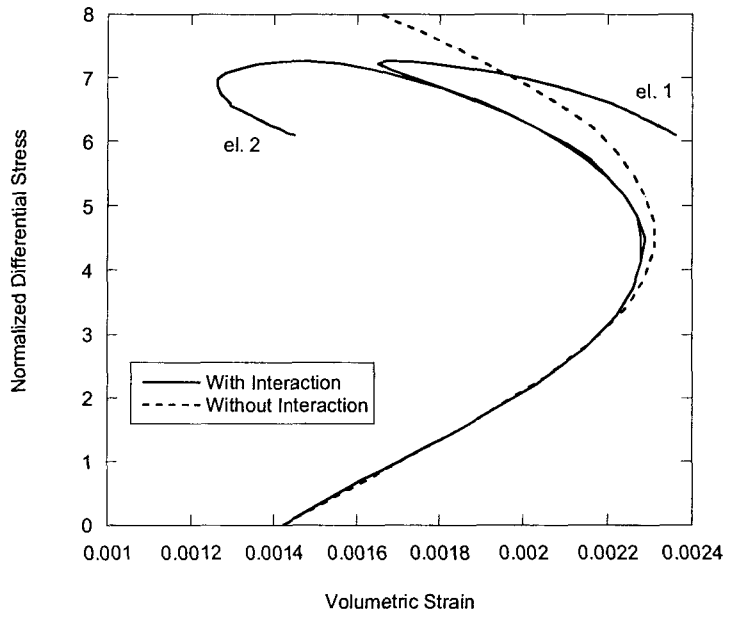

Figure 2.8 Normalized differential stress versus volumetric strain for $\sigma_{11}/\sigma_r = 0.80$.

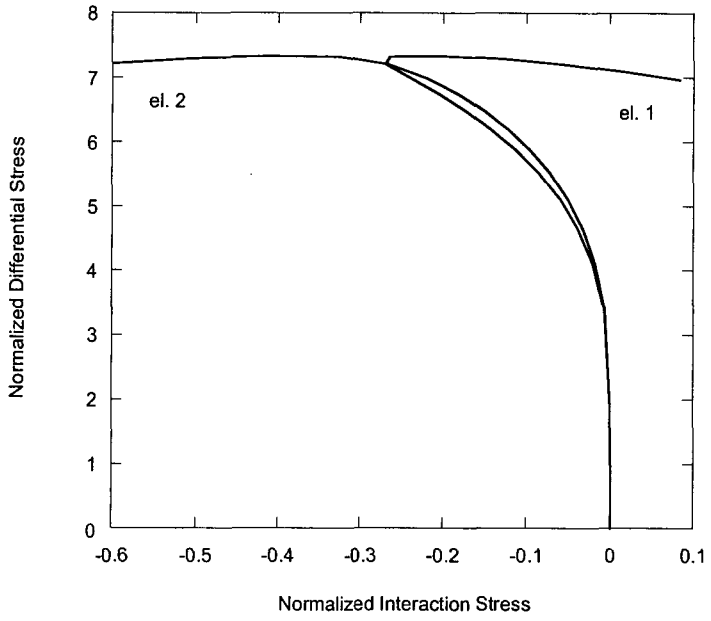

Figure 2.9 Normalized differential stress versus normalized interaction stress for $\sigma_{11}/\sigma_r = 0.80$.

2.3.3.2 Effect of cracks geometry

2.3.3.2.1 Cracks density

The results of simulation for a problem with one group of vertical microcracks for different densities on element No.2 are shown in Figure 2.10. Model parameters are assumed as follows: Length parameter $d = 0.69c_0$ and initial microcracks length $2c_0 = 1.00\ mm$. For the problem with no cracks, there is no critical point and rock sample behaves as an elastic material. However for the problem with microcracks, increasing microcracks density reduces peak axial stress.

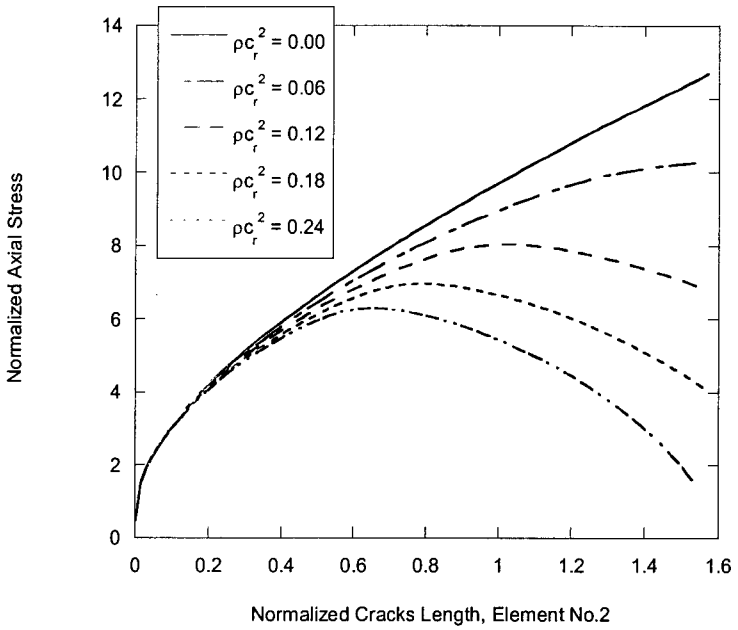

Figure 2.10 Normalized axial stress versus normalized vertical cracks length c/c_r for $\sigma_{11}/\sigma_r = 0.80$.

2.3.3.2.2 Cracks orientation

The biaxial compression test was simulated for the rock sample with one group of microcracks with angle of θ , angle between unit vector normal to the microcrack surface and confining pressure (σ_{11}) , Figure 2.11. The simulation parameters are $\rho\, c_r^2 = 0.24$, $d = 0.69c_0$. With increasing θ, microcracks length corresponding to peak axial stress decreases. And there is no crack growth for θ greater than about 20° (half of initial cracks length is $c_0 = 0.50\ mm$). In other words, active microcracks are oriented in a cone of angle about 20 along the direction of greatest compressive stress σ_1. It can be concluded that the mechanical properties of rocks depend not only on the cracks density but also on the cracks distribution.

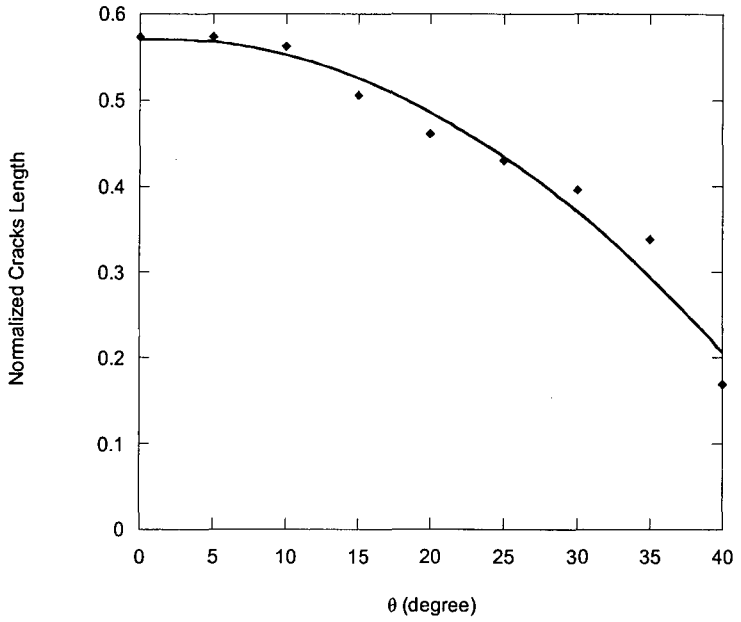

Figure 2.11 Normalized cracks length for peak axial stress versus angle between cracks orientation and axial loading direction for $\sigma_{11}/\sigma_r = 0.80$.

Differential stress versus vertical cracks length c/c_r is shown in Figure 2.12, for two problems: problem with one set microcracks of $\rho_V c_r^2 = 0.24$ (vertical) and another problem with two sets microcracks of $\rho_V c_r^2 = 0.24$ and $\rho_H c_r^2 = 0.12$ (vertical and horizontal), respectively. Other parameters are chosen as $d = 0.69c_0$ and $c_0 = 0.50\ mm$. In case of two sets of microcracks, although horizontal microcracks do not propagate remarkably, however they still have effect on the mechanical properties of brittle materials (Interaction effect). In other words, all microcracks affect mechanical behavior of brittle materials, however the most effective microcracks are oriented in a cone of angle about 20 degree long the axial loading direction.

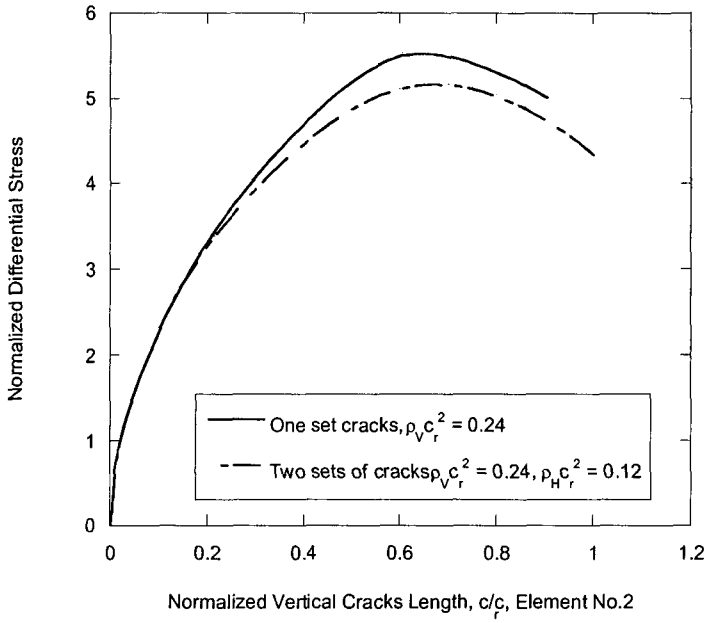

Figure 2.12 Normalized differential stress versus normalized vertical cracks length c/c_r *for* $\sigma_{11}/\sigma_r = 0.80$.

2.3.3.2.3 Initial cracks length

Figure 2.13 shows the evolution of microcracks lengths in element No. 2 for different initial microcracks lengths (c_o). The parameters of model are $\rho\, c_r^2 = 0.12$ and $d = 0.69c_0$ and there is only one group of microcracks (i.e., vertical).With increasing initial cracks length, peak differential stress decreases and this reduction is accelerated with increasing initial cracks length.

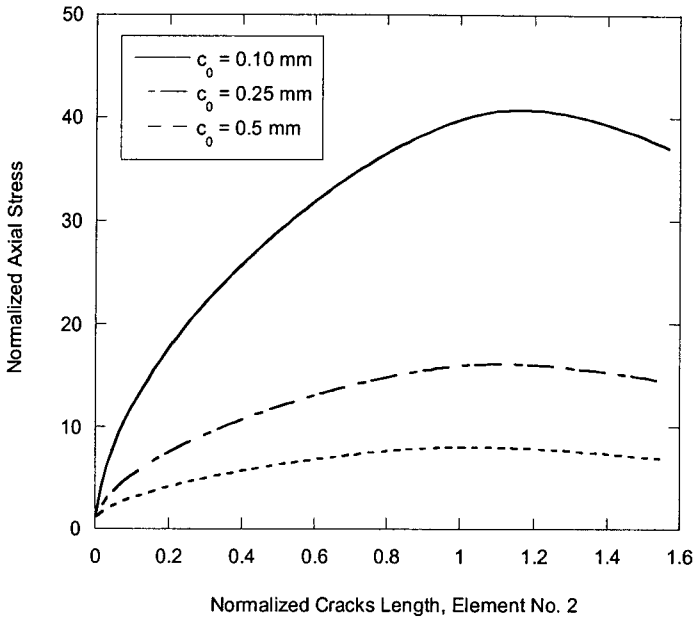

Figure 2.13 Normalized differential stress versus normalized cracks length c/c_r for different initial cracks length, $\sigma_{11}/\sigma_r = 0.80$.

2.4 COMPARISON OF THEORY WITH EXPERIMENTAL RESULTS

We shall illustrate the predictive capability of the proposed model for mechanical behavior of brittle materials. In order to compare the model developed here with rock behavior measured in the laboratory, the results of triaxial compression test on Inada granite and also, microscopic observations of microcrack growth associated with the inelastic deformation are used.

First, Inada granite (i.e., material test) is described briefly. Then, the model parameters are obtained from results of triaxial compression tests. Also, determination of microcracks parameters using thin section of Inada granite (microscopic observation) is explained. Finally, the numerical simulation and experimental data for Inada granite are compared.

2.4.1 Inada granite

Inada granite was sampled from a quarry in Kasama, Ibaraki, Japan. The mean grain size is about 2.0 mm. In spite of the homogenous appearance of Inada granite, three orthogonal planes rift, grain and hardway were detected in the field as reflected by ease or difficulty of fracture in these directions. Pre-existing microcracks are preferentially oriented parallel to the rift and hardway plane (e.g., Sano et al., 1992; Takemura et al., 2003). Inada granite consists of quartz (37%), alkali feldspar (24%), plagioclase (33%), biotite (6%) and some other trace minerals (Suzuki et al. 1990). The intact granite looks fresh (not weathered). When observed under an optical or a scanning electron microscope, however, it was found that biotite is weathered and plagioclase sometimes shows weathering-related porosity along cleavage planes. As has already been noted, Inada granite fails in a two-dimensional fashion in the sense that pre-existing microcracks grow preferentially, parallel to the rift and grain planes.

2.4.2 Model parameters

2.4.2.1 Elasticity parameters E and ν

Laboratory experiments on rock fracture in compression are normally carried out by loading cylindrical specimens. Cylindrical samples 5 cm in diameter and 12 cm long were taken from two blocks of Inada granite, which were cored normal to the rift and the hardway planes. Top and bottom planes of each sample were carefully ground, using an automated grinder, to make them parallel with tolerance of 0.007 mm. After dried in air, the sample was enclosed in heat shrinkable tubing and axial and circumferential extensometers were attached on the central half. Without using any lubricant, the sample was directly mounted on loading platens with the same diameter as that of sample and subjected to a confining pressure ($=\sigma_1$; selected from 0 to 140 MPa) in a triaxial vessel. The samples were axially loaded until the axial stress σ_2 reached the peak axial stress.

The confining pressure versus E_{50} and ν_{50} are plotted as shown in Figures 2.13 and 2.14. E_{50} and ν_{50} were determined from tangent to the axial stress-axial strain and axial stress- lateral strain curves at a stress point corresponding to 50 percent of the peak stress. Since pre-existing microcracks are closed at this stress level, E_{50} and ν_{50} reflect the elasticity parameters of the rock matrix. The mean values of E_{50} and ν_{50}

are 73 GPa and 0.23, respectively.

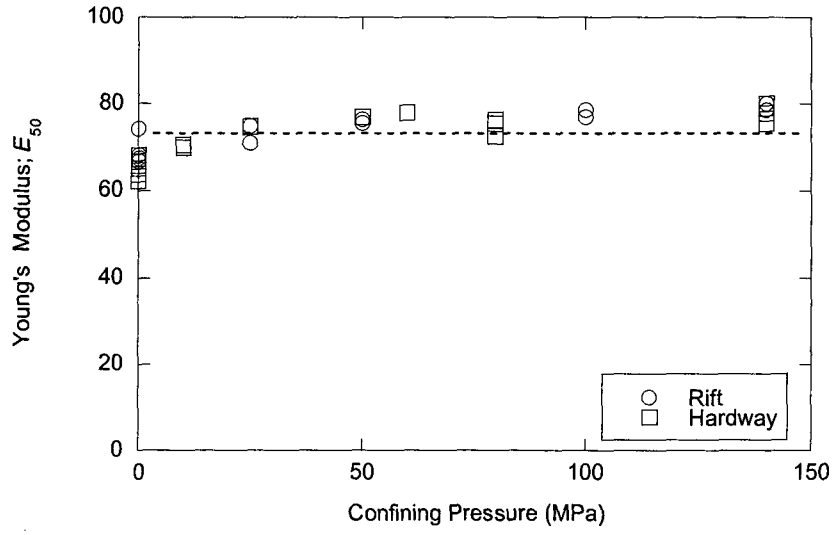

Figure 2.13 E_{50} versus confining pressure for Inada granite.

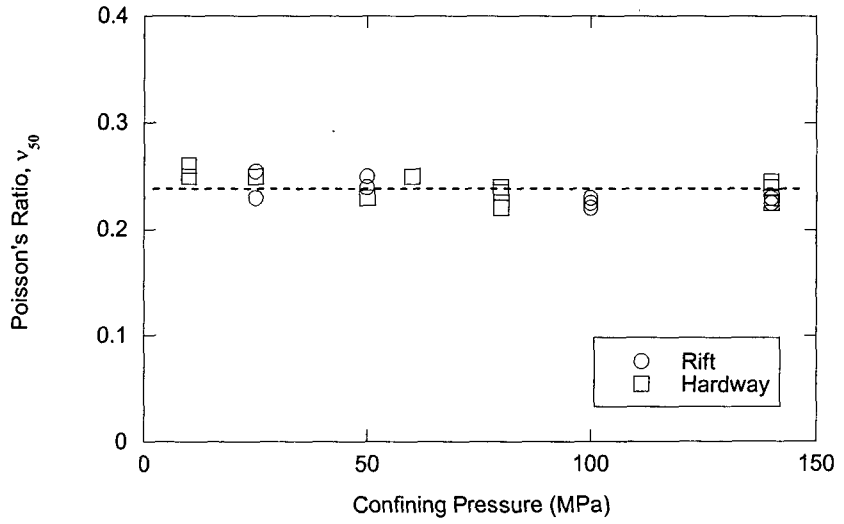

Figure 2.14 ν_{50} versus confining pressure for Inada granite.

2.4.2.2 Length parameter d and fracture toughness K_{IC}

As discussed before, parameter d can be calculated from slope of confining pressure/deviatoric stress graph for initial yield. The problem is how to determine the initial damage point C' on a stress-strain curve. Referring to the suggestion by Brace et al. (1966) that linearity is lost at C' (Fig. 2.15), we tried to locate such a point on the stress-volumetric strain curve. Although we found it very difficult to do with sufficient accuracy, we could still specify such an initial damage point on the stress-volumetric strain curve using a common criterion. The initial damage stresses thus obtained are plotted in Fig. 2.16 as a function of confining pressures σ_{11}. For comparison, the deviatoric stresses at failure are also plotted in the same figure. The data points for the initial damage stresses fall along a straight line, as predicted by Eq. (2.27), and the slope $(d/c_0)^{-1}$ is about 1.48. The length parameter d equals 0.34 mm since c_0 is about 0.5 mm as shown later.

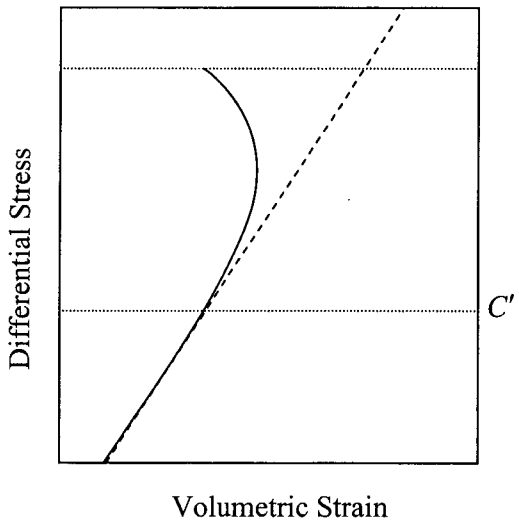

Figure 2.15 Definition of C'

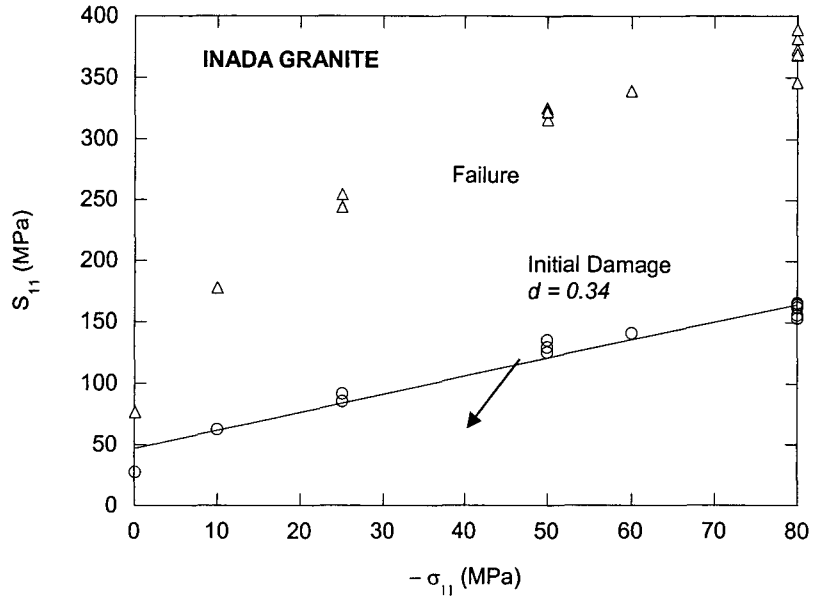

Figure 2.16 Initial damage and failure curves for Inada granite.

One comment is still worth noting here. If the above definition of C' is accepted, the points are located within 35-50% of the peak stress. However, our recent study suggests that the initial damage stresses are within 50-60% of the peak stress. The straight line in Fig. 5.4 should no doubt be shifted upward to some extent, provided a more reliable method is established to determine the initial damage stress. It seems reasonable to think, however, that the slope does not change very much as a result of the correction. Accordingly, we use it in the following analyses. Of course, the fracture toughness K_{IC} can also be determined using S_{11} at $\sigma_{11} = 0$ in Fig. 2.16. Because of the ambiguity discussed above, K_{IC} is set to 2.5 MPam$^{1/2}$ on a tentative basis.

2.4.2.3 Density and length of microcracks

A thin section ($60\mu m$ thick), which was perpendicular to the hardway axes, was prepared from intact sample of Inada granite After taking photograph of thin section, all microcracks were observed under a microscope set up at 100 maginfication in order to trace them out as lines on the photograph. Each trace line, if it was longer than 0.5 mm (cut-off length), was recorded by reading the coordinates of its two ends. These coordinates were used to calculate microcracks lengths. Also, the number of microcracks was individually counted. The microcracks can be classified into four sets depending on their orientations, as follows:

Table 2.1 Model parameters used in numerical simulation for Inada granite.

Parameter	Value(s)			
Young's modulus	$E = 7.3 \times 10^4$ MPa			
Poisson's ratio	$\nu = 0.23$			
Fracture toughness	$K_{IC} = 2.5 MPam^{1/2}$			
Microcracks orientation	Vertical	45°	Horizontal	135°
Initial crack lengths: c_o (mm)	0.56	0.61	0.54	0.40
Number density of microcracks: ρ (mm^{-2})	0.21	0.11	0.43	0.37
Length parameter	$d = 0.34$			

1) Vertical microcracks $(337.5 < \theta \le 22.5$ *or* $157.5 < \theta \le 202.5)$
2) 45 degree microcracks $(22.5 < \theta \le 67.5$ *or* $202.5 < \theta \le 247.5)$
3) Horizontal microcracks $(67.5 < \theta \le 112.5$ *or* $247.5 < \theta \le 292.5)$
4) 135 degree microcracks $(112.5 < \theta \le 157.5$ *or* $292.5 < \theta \le 337.5)$

θ is angle between microcracks surfaces and Rift axes (loading axes), Figure 2.17. For each set of microcracks, initial length $c^{(i)}$ and density $\rho^{(i)}$ were calculated as shown in Table 2.1.

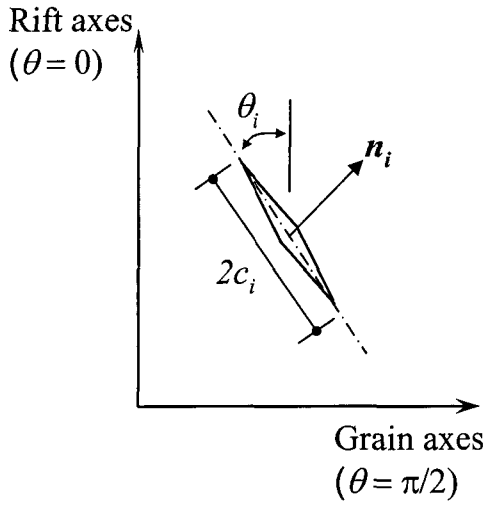

Figure 2.17 Microcracks orientation on thin section (Hardway plane).

2.4.3 Numerical model

Figure 2.18 shows the model used in the numerical simulation for Inada granite which represents two-dimensional plane strain. The boundary conditions are the same as the numerical example in chapter 4. c_r is the reference crack length which is assumed to be 1.00 mm and accordingly the reference stress becomes $\sigma_r = K_{IC} / \sqrt{\pi\, c_r} = 63$ MPa.

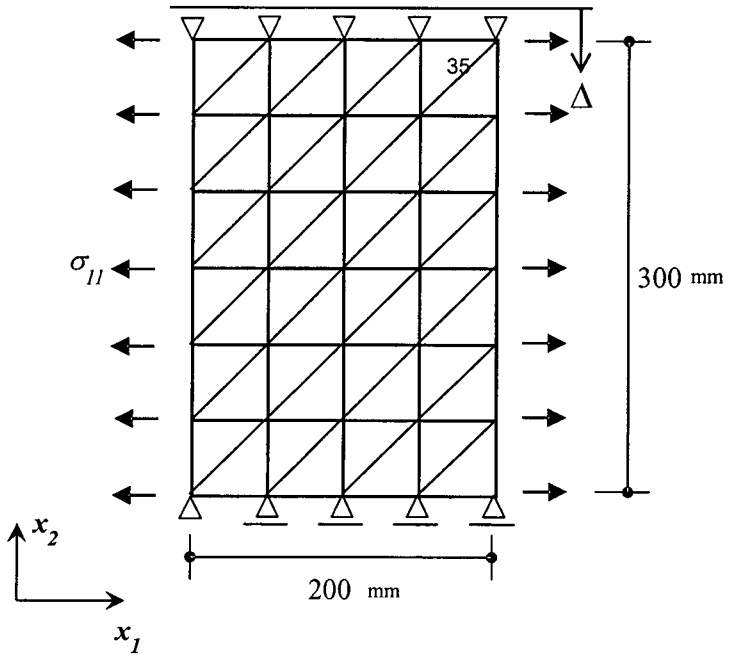

Figure 2.18 Finite element mesh for Inada granite.

In Figure 2.19 the relationship between differential stress, axial strain and lateral strain at three different confining pressures 20, 40 and 60 MPa are shown. With increasing confining pressure, the non-linearity of differential stress-axial strain curve decreases. The reason is, with increasing confining pressure, microcracks opening displacement and consequently the inelastic part of strain which is due to microcracks growth, decrease (Horii and Nemat-Nasser, 1986; Oda et al., 2002a). Also, the relation between the differential stress and the volumetric strain is plotted in Figure 2.20. It can be seen that, as confining pressure increases, the unstable growth of microcracks growth is suppressed (Horii and Nemat-Nasser, 1986). In relation to this point, Oda et al. (2002a) have shown the reduction of unstable crack growth with increasing confining pressure in terms of the first invariant of crack tensor F_0.

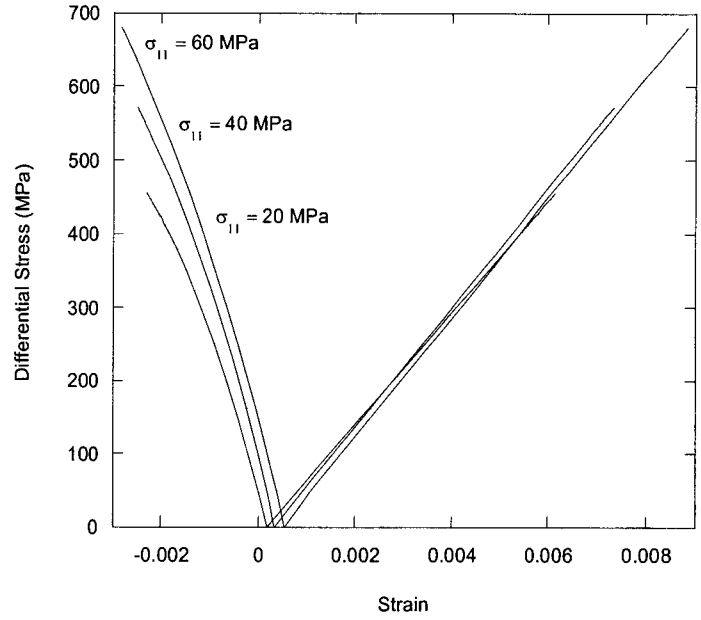

Figure 2.19 Stress-strain curves for different confining pressure.

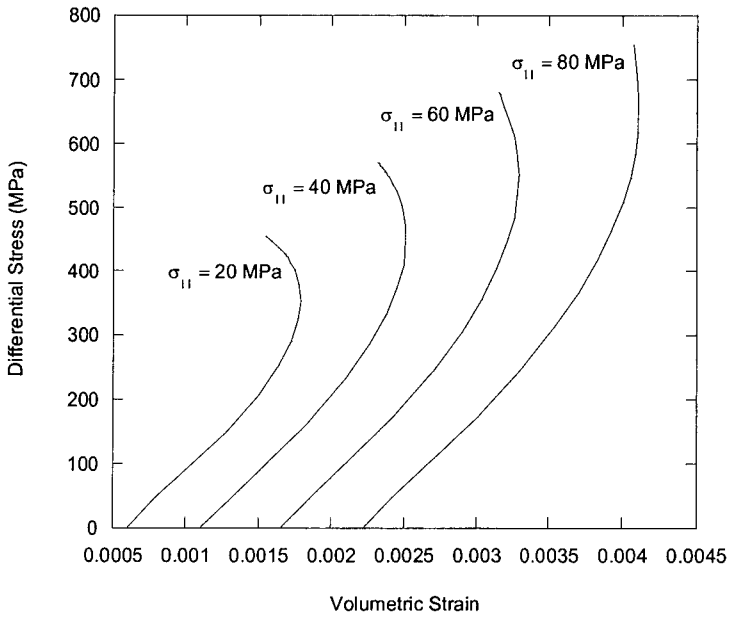

Figure 2.20 Differential stress versus volumetric strain curves for different confining pressure.

Inelastic strain is defined as the maximum departure of the stress-strain curve from the elastic behavior and reflects the total dilation at fracture. Inelastic volumetric strain versus confining pressure is plotted for Inada granite, in Figure 2.21. With increasing confining pressure, the dilation is reduced. This feature agrees with experimental observations (Brace et al., 1966; Zoback and Byerlee, 1975; Gowd and Rummel, 1980; Oda et al., 2002a, b).

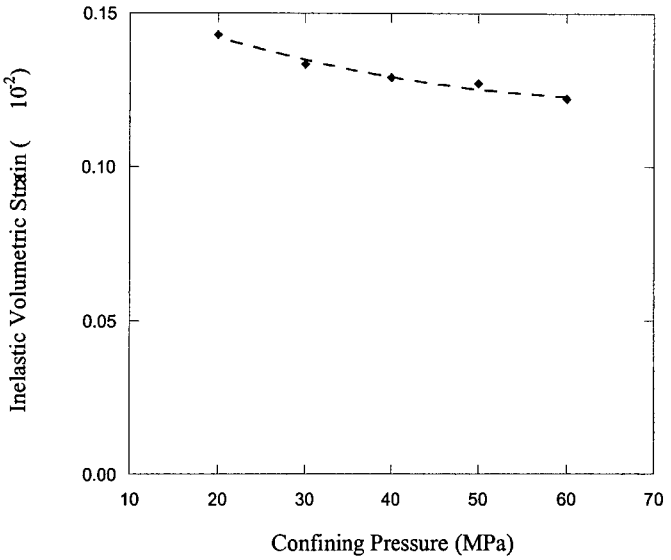

Figure 2.21 Inelastic volumetric strain changes with confining pressure.

2.4.4 Strength of Inada granite

The peak differential stress is plotted as a function of the confining pressure in Fig. 2.22. The failure surface obtained numerically is shown as a solid line in Fig. 5.10, while all the experimental results for Inada granite are plotted as closed circles. It is observed that except for uniaxial tests, the peak differential stresses obtained numerically are in good accordance with the ones observed in the laboratory. In the case of the uniaxial tests, however, the numerical result considerably overestimates the uniaxial strength. The reason is not yet well understood, but is probably because the failure mechanism changes depending on how much confining pressure is applied (e.g., Scholtz, 1968; Hallbauer et al., 1973; Wong, 1982; Horii and Nemat-Nasser, 1986; Oda et al., 2002). Horii and Nemat-Nasser (1985a, b), for example, analyzed crack growth theoretically under axial compression with very small lateral tension. They concluded that tension cracks grow unstably in the axial stress direction, once the crack attains a

critical length. The conclusion is in good accordance with the observation that failure take place due to so-called axial splitting when the confining pressure is less than, say, 5 MPa in Inada granite.

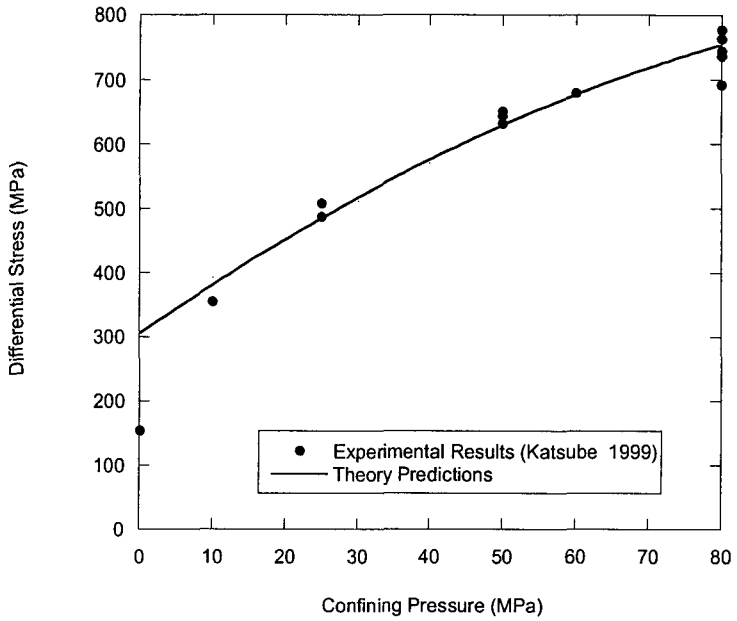

Figure 2.22 Relationship between peak differential stresses and confining pressures for Inada granite.

In relation to this point, Oda et al. (2002) have found that failure in uniaxial stress occurs at a microcrack density much less than that in triaxial tests. This observation also suggests a difference in micromechanism leading to failure (peak stress), depending on the magnitude of the applied pressure.

2.4.5 Microcrack growth

Fig. 2.23 shows how the microcrack length $2c$ changes with increasing applied differential stress. Closed circles were obtained from the triaxial compression tests on Inada granite cariied out at a confining pressure of 80 MPa, while a solid curve was obtained from the numerical calculations under the same condition as that of the triaxial tests. Note that the numerical calculation slightly underestimates the crack length. This fact may arise from the various assumptions in the numerical simulation. For instance, we have assumed that the number density ρ is kept constant while microcracking. In reality, however, the density changes during the loading process. Some neighboring microcracks join each other to give rise to a longer microcrack so that the number density ρ drastically decreases when the differential stress load is close to peak.

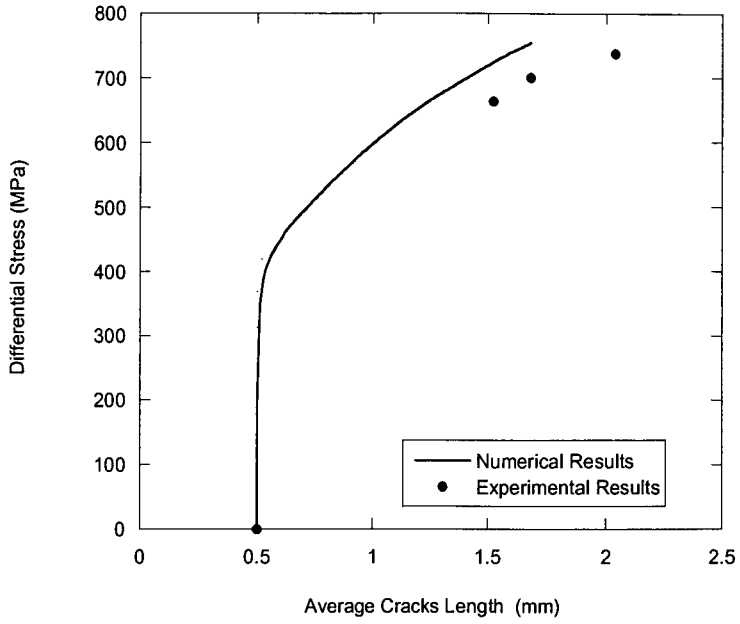

Figure 2.23 Relationship between differential stress and average microcrack length in triaxial compression test of Inada granite at a confining pressure of 80 MPa.

According to the experimental work done by Takemura and Oda (2003), for example, the number density of microcracks decreases from a starting value of $5.9\times10^{-2}\,\mathrm{mm}^3$ to $2\times10^{-2}\,\mathrm{mm}^3$, while Inadad granite is loaded up to 90% of failure stress, and remains almost constant up to failure beyond that point (Fig. 2.24) (The number density in Table 5.1 was obtained from counting the number directly on a two-dimensional section, while the number density reported here was three-dimensionally estimated on a stereology basis. We neglected the change in number density in the present model).

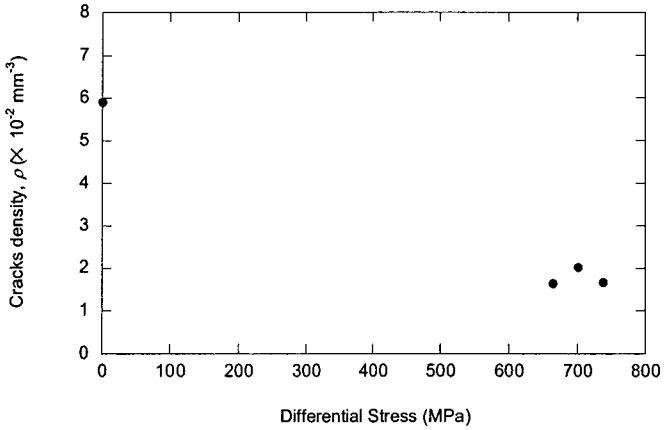

Figure 2.24 Cracks density changes with load increasing for three-dimensional condition, Inada granite (confining pressure is 80 MPa).

2.4.6 Crack density

A tensor quality F_{ij}, called the crack tensor, was introduced as a representative measure for microcrack geometry (Oda, 193, 1984 and 1993). This tensor is expressed as

$$F_{ij} = \frac{1}{V}\sum_{k=1}^{m^{(V)}} S^{(k)} 2c^{(k)} n_i^{(k)} n_j^{(k)} \tag{2.45}$$

where the superscript (k) denotes a kth microcrack in a representative volume element V, $s = \pi c^2$, $m^{(v)}$ is the number of microcracks and n_i is the direction cosines of a unit vector $\boldsymbol{n}$ normal to the microcrack surface (for more details see Oda, 1993; Oda et al., 2002). It is known that the first invariant $F_0 (= F_{11} + F_{22} + F_{33})$ of the crack tensor provides a first-order approximation for estimating quantitatively the microcrack density (not the number density ρ), depending not only on the number density ρ but also on the crack length $2c$.

In Figs. 2.25 and 2.26, the first invariant of the crack tensor F_0 is plotted as a function of the differential stress and crack length, respectively. The solid curve shows the result of numerical calculations. The closed circles represent the results obtained from triaxial tests under a confining pressure of 80 MPa. It can be seen that the crack density increases markedly when the rock is stressed over half of the peak stress, and that the numerical prediction is in a good accordance with the experimental results. We are rather surprised to see the qualitative coincidence in Figs. 2.25 and 2.26 since the numerical simulations are carried out on a two-dimensional basis. Note, however, that there are no experimental data concerning the crack density at the intermediate range where damage growth is accelerated. Accordingly, further experimental studies are needed to reach a final conclusion. A recent study by Takemura and Oda, in which the crack tensor F_{ij} of damaged granite is easily determined by means of elastic wave velocity tests, will be helpful for that purpose.

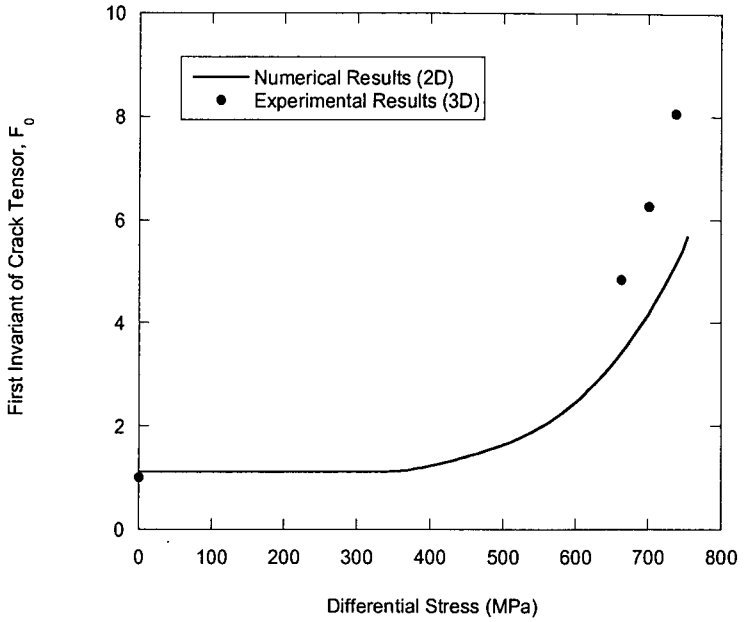

Figure 2.25 Relationship between the first invariant of crack tensor F_0 and differential stress in a triaxial compression test of Inada granite at a confining pressure of 80 MPa.

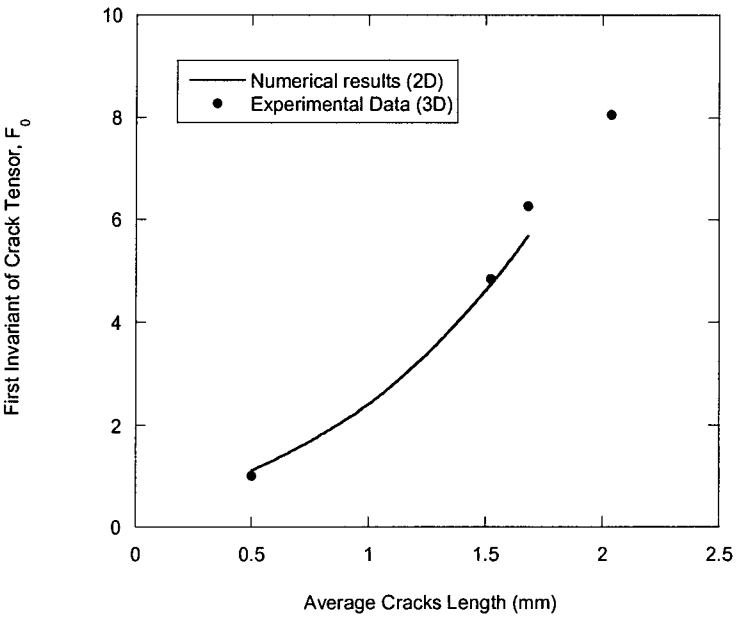

Figure 2.26 Relationship between the first invariant of crack tensor F_0 and average crack length in a triaxial compression test of Inada granite at a confining pressure of 80 MPa.

2.4.7 Strength Anisotropy

Many rocks display strength anisotropy, often due to presence of microcracks. By changing the angle between axial loading and Rift axis φ, triaxial compression test is simulated for a sample of Inada granite under 80 MPa confining pressure (Figure 2.27). As shown in Figure 2.28, strength is strongly dependent to cracks distribution. The minimum strength occurs when the microcracks set with the greatest density exists along the axial loading axis (i.e., grain axes). In Figure 2.29, vertical and horizontal cracks length changes with φ have been plotted. The result shows that only microcracks oriented in a cone of angle about 20 degree along the direction of axial loading are active and do propagate (as discussed in section 2.3.3.2.2).

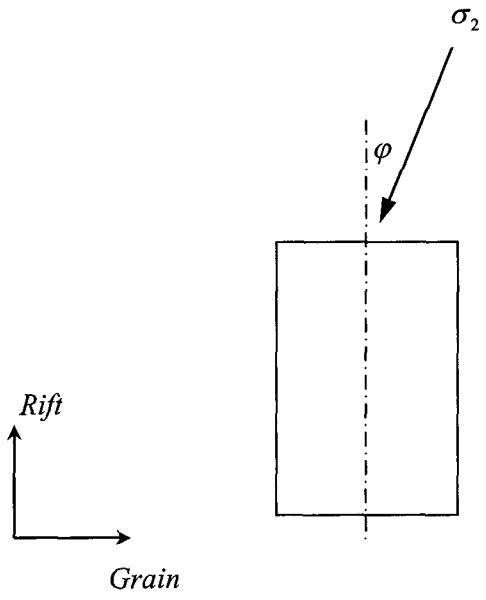

Figure 2.27 Definition of φ

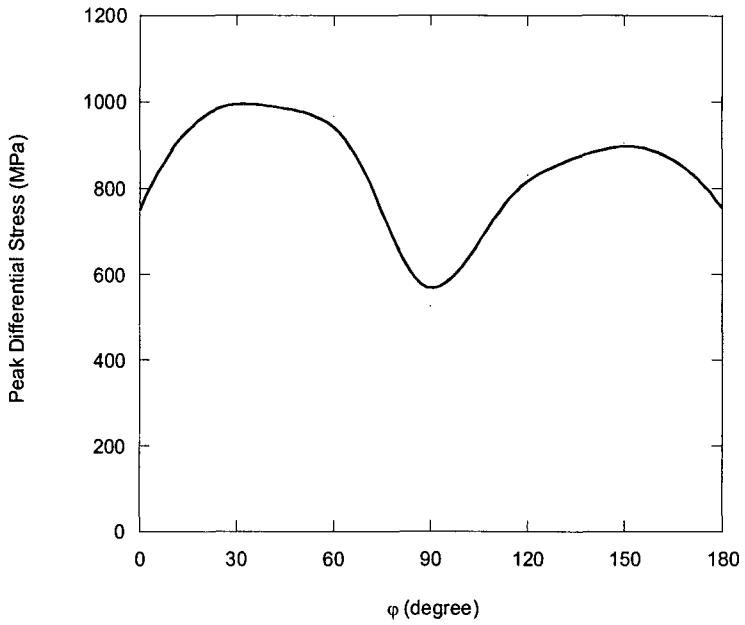

Figure 2.28 Relationship between strength of Inada granite and angle of axial loading with Rift axis (φ).

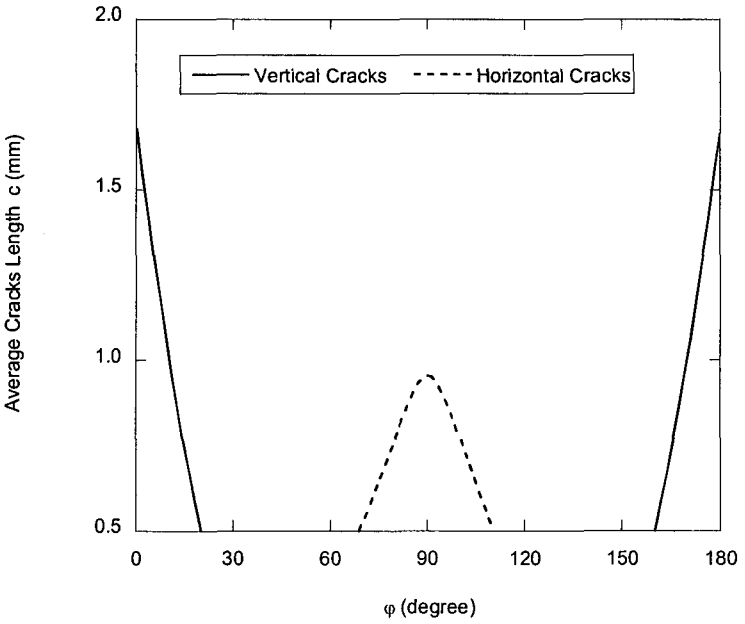

Figure 4.29 Relationship between Vertical and Horizontal cracks length and angle of axial loading with Rift axis (φ).

2.5 CONCLUSIONS

A Micromechanics-based continuum damage model for brittle failure of rock under compression has been proposed to provide a numerical tool for analyzing not only the macro-scale mechanical responses of rock such as strength, but also the microscopic events which take place in association with the inelastic deformation in rock. Special emphasis is placed on how to predict numerically the changes in crack length and crack density during inelastic deformation ending up with brittle failure. If this can be done successfully, the numerical code based on the micromechanics-based continuum damage model can easily be extended to analyze coupling behavior between microcrack growth and the fluid flow through rock. The pre-existing cracks may be randomly distributed or may have an initial preferential distribution. They may be of varying sizes and orientations. The effects of interaction among microcracks are directly taken into account in the constitutive equations (cracks are dealt with together). For considering the interaction effects, the generalized form of Interaction Filed Theory IFT for microcracks with different orientation, was used. A small number of parameters are involved in this model and each one is physically meaningful and can be identified from standard laboratory tests. Note that, in this model, stress-strain relationship at any point depends on the stress and crack geometry at all points in the body. In other words, since the behavior of material depends on the stress and crack geometry at other points, the derived constitutive equation is understood as non-local.

The results show that: In the deformation and failure of brittle rocks, isolated microcrack growth occurs only at relatively low stress. Once numerous microcracks begin to grow, interaction among them starts to play a very important role in the evolution of further microcracking. By considering the interaction effect among microcracks, the behavior of brittle materials can be more realistically modeled, especially in the region near the peak stress. Also, the microcracks oriented in a cone of angle about 20 degrees along the direction of greatest compressive stress, are active and propagate. Although other microcracks do not grow, they affect the mechanicanical properties of rocks and should be considered appropriately. It can be generally understood that the mechanical properties of brittle rocks depend not only on the microcracks density but also on the microcracks distribution.

The peak (failure) stress obtained numerically is in good accordance with the one observed in triaxial compression tests under a confining pressure higher than, say, 10 MPa. In the case of the uniaxial tests, in particular, the numerical model seriously overestimates the uniaxial strength. So-called axial splitting is developed in the laboratory tests of Inada granite under a confining pressure of less than, say, 5 MPa. This means that a major tension crack grows through a sample in the axial stress direction once the crack attains a critical length. In the triaxial compression tests under a higher confining pressure than 10 MPa, on the other hand, failure occurs only when the microcrack density is high enough that coalescence among neighboring microcracks plays a dominant role. The overestimation probably reflects such a difference in micro-mechanism leading to failure (peak stress), depending on the magnitude of the applied confining pressure.

It can be concluded that that the proposed model has a chance of providing a sound basis for predicting with sufficient accuracy crack growth, such as crack length and crack density. However, the present model must still be improved to take into account the following aspects, which are not considered in the present model: First, the real micro-mechanism of crack growth is different from that accepted in the present model, in particular, in the final stage of in-elastic deformation. Second, the number density of microcracks ρ is not constant during the loading process. Some neighboring microcracks join each other to give rise to a longer microcrack so that the number density ρ drastically decreases when the differential stress load increases close to the peak.

REFERENCES

Andreev, G.E. (1995): Brittle failure of rock materials, *Balkema, Rotterdam.*

Atkinson, B.K. (1984): Subcritical crack growth in geological materials, *Journal of Geophysical Research*, Vol. 89, pp. 4077-4114.

Bandis, S.C. (1990): Mechanical properties of rock joints, *Rock Joints*, edited by Barton,

N. and Stephansson, O., Balkema, Rotterdam, pp. 125-140.

Bieniawski, Z.T. (1967): Mechanism of brittle fracture of rock, Part I, II and III, *International Journal of Rock Mechanics and Mining Sciences,* Vol. 4, pp. 395-430.

Brace, W.F., Bomnolakis, E.G. (1963): A note on brittle crack growth in compression, *Journal of Geophysical Research*, Vol. 68, NO. 12, pp. 3709-3713

Brace, W.F., Pauldingm, JR. B.W. and Scholtz, C. (1966): Dilatancy in the fracture of crystalline rocks, *Journal of Geophysical Research*, Vol. 71, NO. 16, pp. 3939-3953.

Broberg, K.B. (1999): Cracks and Fracture, *Academic Press*, U.K.

Cai, M. and Horii, H. (1992): A constitutive model of highly jointed rock masses, *Mechanics of Materials*, 13, pp. 217-246

Chau, K.T., Yang, X. and Wong, R.C.K. (2000): Interactions of a penny-shaped crack with a center of dilatation in an elastic half-space, *Mechanics of Materials*, 32, pp. 645-662.

Chudnovsky, A., Botsis, J. and Kunin, B. (1988): The role of microdefects in fracture propagation process, *Cracking and Damage*, edited by Mazars, J. and Bazant, Z.P., Elsevier, pp. 140-149, pp. 829-840.

Costin, L.S. (1983a): A microcrack model for the deformation and failure of brittle rock, *Journal of Geophysical Research*, Vol. 88, No. B11, pp. 9485-9492

Costin, L.S. (1983b): A microcrack damage model for brittle rock, *Sandia Report* Sand83-1590, sandia National Laboratories, Albuquerque, NM.

Costin, L.S. (1985): Damage Mechanics in the post-failure regime, *Mechanics of Materials,* 4, pp. 149-160

Costin, L. S. (1987a): Time-dependent deformation and failure, *Frcature Mechanics of Rock,* edited by Atkinson, B.K., Academic Press, pp. 167-215.

Costin, L.S. and Stone, C.M. (1987b): Implementation of a finite element damage model for rock, *Constitutive Laws for Engineering Materials, Theory and Applications, Volume II*, edited by Desai, C.S., Krempl, E., Kiousis, P.D. and Kindu, T., Elsevier.

Dey, T.N. and Wang, C.Y. (1981): Some mechanisms of microcrack growth and interaction in compressive rock failure, *Int. J. Rock Mech. Min. Sci. & Geomech. Abstr.*, Vol. 18, pp. 199-209.

Douglass, P.M. and Voight, B. (1969): Anisotropy of granites: A reflection of microscopic fabric, *Geotechnique*, 19, No.3, pp.376-398.

Fang, Z. and Harrison, J.P. (2002): Application of a local degradation model to the analysis of brittle fracture of laboratory scale rock specimens under triaxial conditions, *International Journal of Rock Mechanics and Mining Sciences,* 39, pp. 459-476.

Golshani, A., Takemura, T., Takizawa, A., Kaya, K., Oda, M. and Suzuki, K. (2002), Determination of Oshima granite elastic constants using uniaxial compression tests and crack tensor theory, *The 11th Japan National Symposium on Rock Mechanics*, E-14, 2002.

Hadley, K. (1976): Comparison of calculated and observed crack densities and seismic velocities in westerly granite, *Journal of Geophysical Research*, Vol. 81, NO. 20, pp. 3484-3494.

Hajiabdolmajid, V., Kaiser, P.K. and Martin, C.D. (2002): Modelling brittle failure of rock, *International Journal of Rock Mechanics and Mining Sciences,* 39, pp. 731-741.

Hallbauer, D.K., Wagner, H. and Cook, N. G.. W. (1973): Some observations concerning the microscopic and mechanical behavior of quartzite specimens in stiff, triaxial compression test, *Int. J. Rock Mech. Min. Sci. & Geomech. Abstr.*, 6, pp. 713-726.

Horii, H. and Nemat-Nasser S. (1985): Compression-induced microcrack growth in brittle solids: axial splitting and shear failure, *Journal of Geophysical Research*, 90, pp. 3105-3125.

Horii, H. and Nemat-Nasser, S. (1986): Brittle failure in compression: splitting, faulting

and brittle-ductile transition, *Phil. Trans. R. Soc. Lond.*, A 319, pp. 337-374.

Hoxha, D. and Homand, F. (2000): Microstructural approach in damage modeling, *Mechanics of Materials*, 32, pp. 377-387.

Kachanov, M. (1980): Continuum model of medium with cracks, *J. Eng. Mech. Div.*, 106(EM5), pp. 1039-1051.

Kachanov, M. (1992): Effective elastic properties of cracked solids: critical review of some basic concepts, *Appl. Mech. Rev.*, Vol. 45, No. 8, pp. 304-335.

Kachanov, M. (1994), Elastic solids with many cracks and related problem, *Adv. Appl. Mech.*, 30, pp. 259-445.

Kameda, A. (2002): Elastic wave velocity changes with damage growth in Inada granite, *Bachelor of Science thesis*, Saitama University, Japan.

Krajcinovic, D. and Fonseka, G. U. (1981): The continuous damage theory of brittle materials, *J. Appl. Mech.*, 48, pp. 809-815.

Kranz, R. L. (1979): crack growth and development during creep of Barre granite, *Int. J. Rock Mech. Min. Sci. & Geomech. Abstr.*, 16, pp. 23-35.

Kranz, R. L. (1983): Microcracks in rocks: A review, *Tectonophysics*, 100, pp. 449-480.

Li, H.B., Zhao, J. and Li, T.J. (2000): Micromechanical modeling of the mechanical properties of a granite under dynamic uniaxial compressive loads, *International Journal of Rock Mechanics and Mining Sciences*, 37, pp. 923-935.

Liao, J.J., Hu, T.-B. and Chang, C.-W. (1997): Determination of dynamic elastic constants of transversely isotropic rocks using a single cylindrical, *International Journal of Rock Mechanics and Mining Sciences,* Vol. 34, No.7, pp. 1045-1054.

Miura, K., Okui, Y. and Horii, H. (2003): Micromechnanics-based prediction of creep failure of hard rock for long-term safety of high-level radioactive waste disposal system, *Mechanics of Materials*, 25, pp. 587-601

Moore, D. E. and Lockner, D.A. (1995): The role of microcracking in shear-fracture propagation in granite, *Journal of Structural Geology*, No. 17(1), pp. 95-114.

Murakami, S. (1988): Mechanical modeling of material damage, *Journal of Applied Mechanics*, Vol. 55, pp. 280-286.

Nemat-Nasser, S. (1985): Discussion to "Geometrical probability approach to the characterization and analysis of microcracking in rocks", *Mechanics of Materials*, 4, pp. 227-281.

Nemat-Nasser, S. and Obata, M. (1988): A microcrack model of dilatancy in brittle materials, *Journal of Applied Mechanics*, Vol. 55, pp. 24-35.

Oda, M. (1982): Fabric tensor for discontinuous geological materials, *Soils and Foundations*, Vol. 22, No. 4, pp. 96-108.

Oda, M. (1983): A method for evaluating the effect of crack geometry on the mechanical behavior of cracked rock masses, *Mechanics of Materials*, 2, pp. 163-171.

Oda, M. (1984a): Similarity rule of crack geometry in statistically homogenous rock masses, *Mechanics of Materials*, 3, pp. 119-129.

Oda, M., Suzuki, K. and Maeshibu T. (1984b): Elastic compliance for rock-like materials with random cracks, *Soils and Foundations*, 24, pp. 27-40.

Oda, M. (1985): Permeability tensor of discontinuous rock masses, *Geotechnique*, 35, No. 4, pp. 483-495.

Oda, M. (1986): An equivalent comtinuum model for coupled stress and fluid flow analysis in jointed rock masses, *Water Resources Research*, Vol. 22, No.13, pp. 1845-1856.

Oda, M., Yamabe, T. and Kamemura, K. (1986): A crack tensor and its relation to wave velocity anisotropy in jointed rock masses, *Int. J. Rock Mech. Min. Sci. & Geomech. Abstr.*, Vol. 23, pp. 387-397.

Oda, M. and Hatsuyama, Y. (1987): Numerical experiments on permeability tensor and its application to jointed granite at Stripa mine, Sweden, *Journal of Geophysical Research*, Vol. 92, No. B8, pp. 8037-8048.

Oda, M. (1988): An experimental study of the elasticity of Mylonite rock with random cracks, *Int. J. Rock Mech. Min. Sci. & Geomech. Abstr.*, Vol. 25, No. 2, pp. 59-69.

Oda, M. (1993a): Modern developments in rock structure characterization, *in compressive Rock Engineering*, Vol. 1, edited by J.A.Hudson, pp. 185-200.

Oda, M., Yamabe, T., Ishizuka, Y., Kumasaka, H., Tada, H. and Kimura K. (1993b): Elastic stress and strain in jointed rock masses by means of crack tensor analysis, *Rock Mechanics and rock Engineering*, 26(2), pp. 89-112.

Oda, M., (1995): Fundamentals of Geomechanics, *Textbook*, Saitama university, Japan.

Oda, M., Kanamaru, M. and Iwashita, K. (1996): The effect of crack geometry on hydrodynamic dispersion in cracked media, *Soils and Foundations*, Vol. 36, No. 2, pp. 69-80.

Oda, M. and Iwashita, K. (1999): Mechanics of Granular Materials, *Balkema*, Rotterdam, Netherlands.

Oda, M., Katsube, T. and Takemura, T. (2002a): Microcrack evolution and brittle failure of Inada granite in triaxial compression tests at 140 MPa, *Journal of Geophysical Research*, Vol. 107, NO. B10.

Oda, M., Takemura, T. and Aoki, T. (2002b): Damage growth and permeability change in triaxial compression tests on Inada granite, *Mechanics of Materials*, 34, pp. 313-331.

Okui, Y. (1993): A microcrmechanics-based continuum theory for localization phenomena, *Doctoral thesis*, University of Tokyo, Japan.

Okui, Y., Horii, H. and Akiyama, N. (1993): A continuum theory for solids containing microdefects, *Int. J. Eng Mech.*, Vol. 31, No. 5, pp. 735-749.

735-749.

Okui, Y. and Horii H. (1997): Stress and time-dependent failure of brittle rocks under compression: A theoretical prediction, *Journal of Geophysical Research*, Vol. 102, NO. B7, pp. 14869-14881.

Ortiz, M. and Popov, Egor P. (1982): Plain concrete as a composite material, *Mechanics of Materails*, 1, pp. 139-150.

Ortiz, M. (1985): A constitutive theory for the inelastic behavior of concrete, *Mechanics of Materails*, 4, pp. 67-93.

Pan, Y.-W. and Wen, B.-H. (2001): Constitutive model for the continuous damage of brittle rock, *Geotechnique*, 51, No. 2, pp. 155-159.

Rodrigues, F.P. (1966): Anisotropy of granite, Proceeding of the first congress ISRM, Vol. 1, pp. 721-731.

Rudnicki, J.W. and Chau, K.T. (1996): Multiaxial response of a microcrack constitutive model for brittle rock, *Rock Mechanics*, Balkema, Rotterdam, pp.1707-1714

Sanford, R.J. (2003): Principles of fracture mechanics, *Prentice Hall*, USA.

Sano, O., Kudo, Y. and Mizuta, Y. (1992a): Experimental determination of elastic constants of Oshima granite, Barre granite, and Chelmsford granite, *Journal of Geophysical Research*, Vol. 97, NO. B3, pp. 3367-3379

Sano, O. and Kudo, Y. (1992b): Relation of fracture resistance to fabric for granitic rocks, PAGEOPH, Vol. 138, No.4, pp. 656-677.

Scholtz, C. H. (1968): Microfracturing and the inelastic deformation of rock in compression, *Journal of Geophysical Research*, 73, No.4, pp. 1417-1432.

Scholtz, C.H.(2002): The mechanics of earthquakes and faulting, *Cambridge University,* UK.

Shao, J.F., Hoxha, D., Bart, M., Homand, F., Duveau, G., Souley, M. and Hoteit, N. (1999): Modelling of induced anisotropic damage in granites, *International Journal of Rock Mechanics and Mining Sciences*, 36, pp. 1001-1012

Shao, J.F. and Rudnicki, J.W. (2000): A microcrack-based continuous damage model for brittle geomaterials, *Mechanics of Meterials*, 32, pp. 607-619

Sprunt, Eve S. and Brace, W.F. (1974): Direct observation of microcavities in crystalline rocks, *Int. J. Rock Mech. Min. Sci. & Geomech. Abstr.*, Vol. 11, pp. 139-150.

Suzuki, K., Oda, M., Yamazaki, M. and Kuwahara, T. (1998): Permeability changes in granite with crack growth during immersion in hot water, *Int. J. Rock Mech. Min. Sci.*, Vol. 35 (7), pp. 907-921.

Tajima, H. (1996): A study of continuum theory accounting for microstructure, *Master of Science thesis*, Saitama University, Japan.

Takemura, T. (2002): Experimental study on brittle failure mechanism of granitic rocks based on microcrack evolution, *Doctoral thesis*, Saitama University (in Japanese).

Takemura, T. and Oda. M. (2002a): Microcrack geometry change in brittle failure of Inada granite, 11th Interior Symposium on Rock Mechanics in Japan (in Japanese).

Takemura, T. and Oda, M. (2002b): Three-dimensional fabric analysis of microcracks associated with brittle failure of granitic rocks, *Jour. Geol. Soc. Japan*, Vol. 108, No.7, pp. 453-464 (in Japanese).

Takemura, T., Golshani, A., Oda, M. and Suzuki, K. (2003): Preferred orientation of open microcracks in granite and their relation with anisotropic elasticity, *International Journal of Rock Mechanics and Mining Sciences*, 40, pp. 443-454.

Takemura, T., Oda, M.: Streology-based fabric analysis of microcracks in damaged granite, *Tectonophysics* 387, pp.131-150.

Tapponnier, P. and Brace, W.F. (1976): Development of stress-induced microcracks in Westerly granite, *Int. J. Rock Mech. Min. Sci. & Geomech. Abstr.*, Vol. 13, pp. 103-112.

Wang, J.G., Ichikawa, Y. and Leung, C.F. (2003): A constitutive model for rock interfaces and joints, *International Journal of Rock Mechanics and Mining Sciences,* 40, pp. 41-53.

Wawersik, W. R. and Brace, W. F. (1971): Post-failure behavior of a granite and diabase, *Rock Mechanics*, 3, pp. 62-85.

Wong, T.-F. (1982): Micromechanics of faulting in Westerly granite, *Int. J. Rock Mech. Min. Sci. & Geomech. Abstr.*, Vol. 19, pp. 49-64.

Wong, R. H. C., Chau, K. T. and Wang, P. (1996): Microcracking and grain size effect in Yuen Long Mrbles, *Int. J. Rock Mech. Sci. & Geomech. Abstr.*, 33, No. 5, pp. 479-485.

Zhao, Y. (1998): Crack pattern evolution and a fractal damage constitutive model for rock, *International Journal of Rock Mechanics and Mining Sciences,* Vol. 35, No.3, pp. 349-366.

Chapter 3

Long-term Behavior of Brittle Rocks

3.1 INTRODUCTION

The use of underground facilities such as waste reservoirs and power station caverns is increasing. However, excavation of such spaces results in a change in stress distribution; the changes alter the mechanical properties of rock mass such as strength and deformability, and the hydraulic conductivities and hence influence contaminant pathways.

Depending on mechanical host rock properties, the stress redistribution may lead to the development of a plastic zone around the space, termed as the excavation disturbed zone (EDZ). The hydro-mechanical behavior of EDZ around underground repositories is a major concern in assessing the safety of these geotechnical barriers. For example, EDZ, which is commonly associated with increased permeability, constitutes a potential risk to the effectiveness of isolating high-level nuclear waste from the environment.

In the past, EDZ was studied by various means, particularly in the field (e.g., Meglis et al.; Souley et al., 2001; Wong et al., 2002; Martino and Chandler, 2004; Read, 2004). For example, Meglis et al. (2001) measured ultrasonic wave velocities within a 1 m deep shell around one quadrant of the Mine-By tunnel at Canada's Underground Research Laboratory during excavation. Their measurements suggested that damage growth is most concentrated in the material immediately adjacent to the tunnel, extending more deeply into the rock in the side walls. Martino and Chandler (2004)

studied the EDZ at the Underground Research Laboratory (URL) in the Lac du Bonnet granite batholith in southern Manitoba, Canada. They measured the properties of the damage zone surrounding the excavation, and found that the *in situ* stress, the tunnel shape and its orientation relative to the maximum stress, excavation method, changes in pore pressure, and the creation of nearby excavations all affect the development of EDZ.

Unfortunately, however, it must be realized that such experimental approaches, in spite of their great importance, cannot be effectively used to predict long-term behavior of EDZ, which might end up with tunnel collapse. In order to overcome this difficulty, some numerical models have been developed by numerous authors (i.e., Adhikary and Dyskin, 1997; Hommand-Etienne et al., 1998; Potyondy and Cundall, 1998; Souley et al., 2001; Fakhimi et al., 2002; Hou, 2003; Chen et al., 2004; Mitami and Detournay, 2004). Hommand-Etienne et al. (1998), for example, proposed a model for numerically analyzing the damage zone around an underground opening excavated in brittle rocks, and found that the highly damaged zones are formed in association with the zones of highly compressive stress. Fakhimi et al,(2002) simulated a biaxial test on a rectangular prism of the Berea sandstone containing a circular opening, and observed that the damage zone started to develop from the side walls of the opening where the compressive stresses were large. Chen et al. (2004) studied the numerically time-dependent behavior of rock around underground excavations in the Shanxai Yellow River Diversion Project. They concluded that the damage zone in the vicinity of side walls is larger than in that of the roof and floor. They successfully investigated how deformation accumulates around a tunnel over time. However, they did not discuss how microcracks grow as a function of time around the excavation. In all honesty, there is very little knowledge on the actual time-dependent development of EDZ arising from stress-induced and time-dependent microcracking in the surrounding rock environment. Considering underground storage of hazardous waste, sufficient knowledge on this issue is crucial because contaminants may migrate through a network of thus induced microcracks.

In this chapter, the micromechanics-based continuum damage model, which was

originally proposed by Golshani et al (2006) for the analysis of short-term microcracking in brittle rocks under compression, is extended to analysis the long-term (creep) microcracking of brittle rocks under compression. Subsequently, the model is applied to the creep tests on Inada granite to assess whether creep behaviors are successfully simulated, and to confirm that the parameters for describing sub-critical microcrack growth can be experimentally determined. Finally, the developed model is applied to simulate the time-dependent development of EDZ around a circular tunnel in terms of the model parameters for Inada granite.

3.2 GOVERNING EQUATIONS

The governing equations for the long-term behavior of brittle rocks are the same equations as given in the previous chapter except for the microcrack growth law which is explained in this section.

Crystalline rocks such as granite fail as a result of initiation and growth of microcracks (e.g., Wawersik and Brace, 1971; Kranz, 1979; Atkinson 1984). When a tunnel is excavated in a crystalline rock at great depth, say 1,000 m, microcracking may occur around the excavation by two mechanisms; (i) short-term (stress-induced) microcracking and (ii) long-term (time-dependent) microcracking, both of which are no doubt related to the formation of EDZ around the tunnel. short-term microcracking occurs when the stress in the vicinity of a microcrack is large enough that the stress intensity factor K_I surpasses the fracture toughness K_{IC}. On the other hand, time-dependent microcracking occurs stably under a constant loading. Importantly, time-dependent microcracking, called sub-critical crack growth, can take place even if the stress intensity factor K_I at the microcrack tip is below the fracture toughness K_{IC}.

In order to incorporate long-term microcracking in the proposed model explained in previous chapter, it is assumed, as usual, that the microcrack growth rate dc/dt is related to the stress intensity factor (e.g., Martin, 1972; Atkinson, 1980; Costin and Mecholsky, 1983; Okui et al., 1997). Following the suggestion by Atkinson (1984),

we use the following expression:

$$dc/dt = A(K_I / K_{IC})^n \tag{3.1}$$

where A is a parameter reflecting environmental conditions such as humidity and temperature, and n is the so-called sub-critical microcrack growth index. Typical values of n range from 30 to 69 for granitic rocks (Atkinson, 1984). Unfortunately, in spite of the great importance, little information is available on the parameter A.

3.3 NUMERICAL ANALYSIS METHOD

The procedure of discretization by finite element method is the same as one shown in the previous chapter, and thus only time-integration scheme is explained briefly in this chapter. After the short-term behavior of the material is computed by the numerical analysis method, Euler method is used to allow the solution to be advanced from time $t^{(s)}$ to time $t^{(s+1)} = t^{(s)} + \Delta t^{(s)}$, where superscripts (s) and $(s+1)$ denote successive times and $\Delta t^{(s)}$ is the time interval. In this method, the mean rate of change of time-dependent variables over the time interval is taken as the value at the beginning of the interval. Thus, from the microcrack growth law (Eq. (3.1)), the increment of the damage parameter (the length of microcracks) occurring during time step $\Delta t^{(s)}$ is obtained as

$$\Delta c^{(s)} = A(K_I / K_{IC})^n \Delta t^{(s)} \tag{3.2}$$

where mode I stress intensity factor K_I is evaluated from equation (2.6) using the stress $\bar{\sigma}^{(s)}$, the pseudotraction $\bar{\sigma}^{P(s)}$ and the damage parameter $\bar{c}^{(s)}$ at time $t^{(s)}$. The total damage parameter $\bar{c}^{(s+1)}$ at time $t^{(s+1)}$ is calculating by adding the incremental value to the previous total value:

$$\bar{c}^{(s+1)} = \bar{c}^{(s)} + \Delta\bar{c}^{(s)} \tag{3.3}$$

After all cracks lengths in each element are calculated, stress $\bar{\sigma}^{(s+1)}$, strain $\bar{\varepsilon}^{(s+1)}$ and displacement $\bar{u}^{(s+1)}$ at time $t^{(s+1)}$ are obtained by solving stiffness equation induced from conventional finite element procedure.

3.4 DETERMINATON OF PARAMETERS

All the parameters involved in the micromechanics-based continuum damage model, except for sub-critical microcrack growth parameters A and n, were chosen in reference to the study on the short-term behaviors of Inada granite (Table 2.1).

The double torsion test is a standard method to obtain the sub-critical microcrack growth index n. It should be noted, however, that there are rather large differences in the values of n, even when the same rock is tested in different laboratories. The sub-critical microcrack growth indexes of Westerly granite, for instance, range from 35.9 to 69 (Atkinson 1984). Sano and Kudo (1992b) reported values of Inada granite ranging from 18 to 41, which were determined at the stress intensity factor of $1\,MPa\sqrt{m}$. In our simulation, we had to determine the sub-critical microcrack growth parameters (i.e., n and A) such that the numerical results of time to failure vs. creep stress ratio curve could be fitted to the same relation experimentally determined for Inada granite. It is found, as will be discussed later, that by using $n = 50$ and $A = 2.0\times10^{-23}$, we can fit the numerical results to experimental data.

3.5 NUMERICAL SIMULATION OF BIAXIAL TESTS

Two-dimensional analyses were carried out using the finite element mesh and boundary conditions as shown in Fig. 3.1. The axial compressive stress σ_{22} is increased, while keeping the lateral compressive stress σ_{11} constant, until the differential stress $(\sigma_{22}-\sigma_{11})$ reaches the desired value. In this process, some stress-induced microcracks grow when the stress intensity factor K_I at crack-tips reaches the fracture toughness K_{IC}. After that, the applied differential stress $(\sigma_{22}-\sigma_{11})$ is held constant until failure occurs (creep analysis). For convenience, $CSR = (\sigma_{22}-\sigma_{11})/(\sigma_{22}-\sigma_{11})_{max}$ is called the creep stress ratio where $(\sigma_{22}-\sigma_{11})_{max}$ is the maximum differential stress obtained from a short-term analysis.

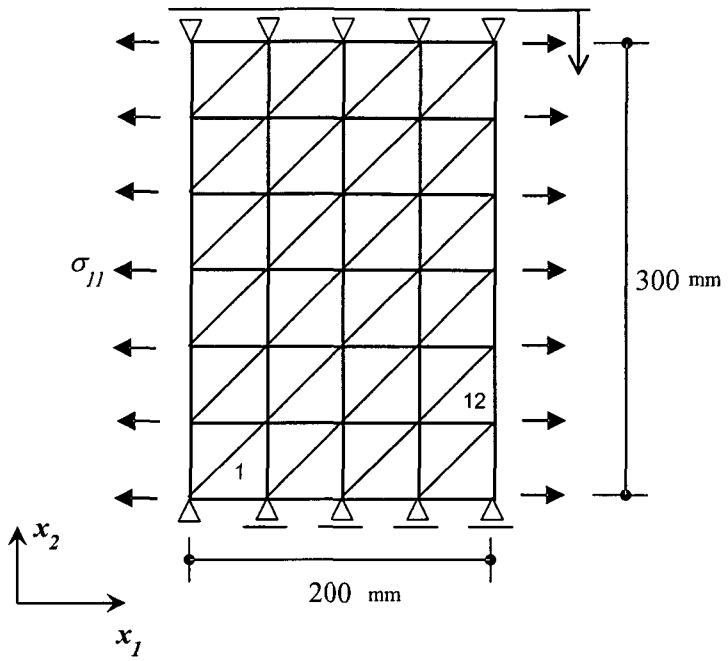

Figure 3.1 Finite element mesh for Inada granite.

Using the present micromechanics-based continuum damage model, many creep tests were run on a computer. Three examples at creep stress ratios CSR of 0.96, 0.94 and 0.92 under a confining pressure σ_{11} of 40 MPa were chosen. In Fig. 3.2, the volumetric strain ε_v calculated by the present model is shown as a function of the elapsed time for an element (Number12). The volumetric strain versus time relationship can be distinguished into three successive stages; (i) primary creep, (ii) secondary creep, and (iii) tertiary creep, which are commonly observed in a laboratory creep test. After the tertiary creep, the sample ends up with creep failure. These three creep stages reflect three different stages of microcrack growth as shown in Fig. 3.3, in which microcrack length is plotted as a function of the elapsed time. It is clear that the tertiary creep is closely linked to the accelerated (unstable) propagation of microcrack length, which ends up with creep failure as a result of the infinite growth.

Fig. 3.4 shows the elapsed time to creep failure as a function of the creep stress ratio ranging from 0.9 to 0.98. The broken, solid and dotted lines correspond to the calculations with parameter values of $A = 2.0\times10^{-22}, 2.0\times10^{-23}$, and 2.0×10^{-24} respectively. It should be noted that the parameter A is changed by keeping the sub-critical microcrack growth index n constant. The line moves upward with increasing

values of parameter A. The sub-critical microcrack growth index n, on the other hand, controls the slope in that relation. The closed triangles in the figure, which are experimental data from the creep test on Inada granite, will be discussed later.

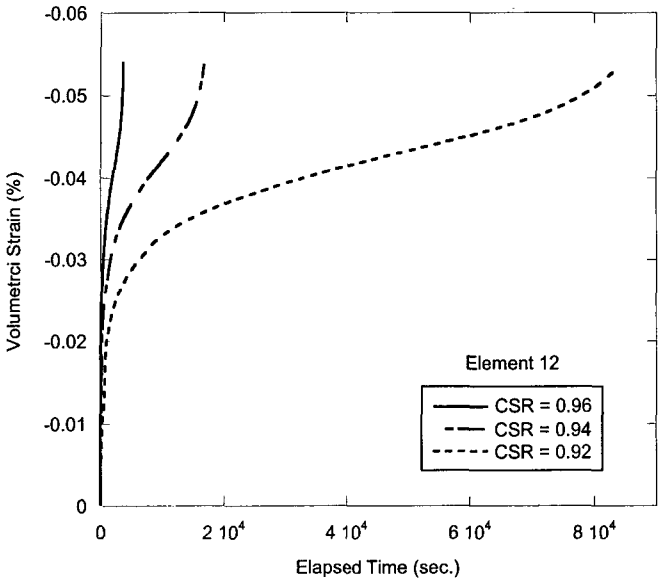

Figure 3.2 Elapsed time vs. volumetric strain of element 12 at three different creep stress ratios CSR (i.e. 0.96, 0.94 and 0.92) under a confining pressure σ_{11} of 40 MP

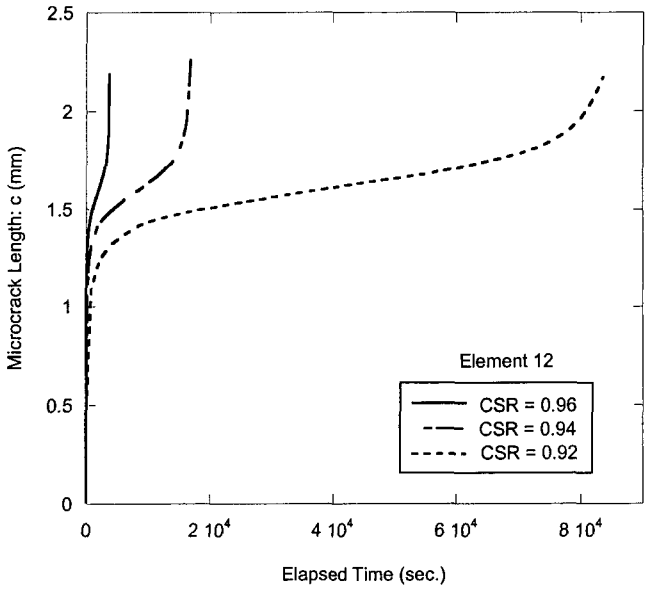

Figure 3.3 Time-dependent crack length growth in element 12 at three different creep stress ratios CSR (i.e. 0.96, 0.94 and 0.92) under a confining pressure σ_{11} of 40 MPa

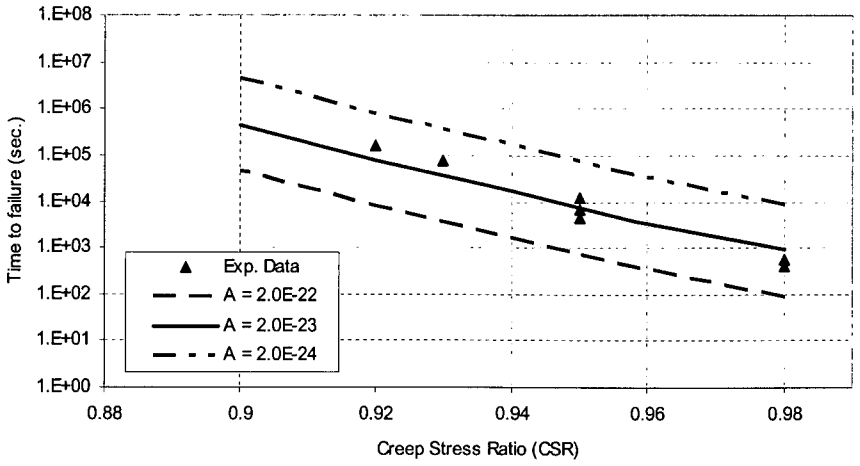

Figure 3.4 Creep stress ratio vs. time to failure at confining pressure of 40 MPa for Inada granite under dry conditions

3.6 LONG-TERM BEHAVIOR IN CREEP TESTS OF INADA GRANITE

3.6.1 Testing procedures

Cylindrical samples, 5cm in diameter and 12cm long, were taken out of blocks quarried from the same site, and the top and bottom surfaces of each sample were carefully ground, using an automatic grinder, to make them parallel within a tolerance of ±0.0035 mm. In order to check the effect of moisture conditions on time-dependent behaviors of Inada granite, seven samples were dried in a desiccator for over a week, and eight samples were immersed in water subjected to a vacuum pressure for the same period.

Each sample thus obtained was subjected to a confining pressure σ_{11} of $40MPa$ at room temperature, and was axially loaded at a constant circumferential extension rate of

-5×10^{-4} mm/s until the differential stress reached a specified value of the creep stress ratio CSR. Subsequently, the differential stress was kept constant until creep failure occurred. The elapsed time to failure was recorded. The whole process was fully controlled by means of a high stiffness loading frame of MTS 815 and a feedback system using signals from a circumferential extensometer.

The creep stress ratio CSR was chosen from a rather limited range from 0.92 to 0.98. If CSR was set below 0.9, the elapsed time to failure might be over one month. This is out of the capacity of the present testing machine.

3.6.2 Experimental results

3.6.2.1 Creep tests on dry Inada granite

Fig. 3.5 shows two examples of creep tests, which were run at CSR = 0.95 and 0.93 under a confining pressure σ_{11} of 40 MPa. The volumetric strains ε_v measured during creep tests are shown as a function of the elapsed time up to failure. Three successive stages of (i) primary creep, (ii) secondary creep, and (iii) tertiary creep can be clearly distinguished in a laboratory creep test. However, the volumetric strain is much bigger in the laboratory test (Fig. 9) than in the numerical calculations (Fig. 6). There might be several reasons to explain the discord between Figs. 3.5 and 3.2 for example, the interaction effects among microcracks on the constitutive relationships were neglected in the present model. Also, the model is two-dimensional, whereas the experimental results are for creep laboratory tests of cylindrical samples. More importantly, in the calculation of the inelastic strain, we only considered inelastic strain due to the changes in microcrack displacement caused by the applied loads. In relation to this point, Nemat-Nasser and Obata (1998) modeled dilatancy in brittle rock successfully. In their model, inelastic strain due to microcrack opening and slip together with inelastic strain due to microcrack displacement caused by applied stresses were taken into account.

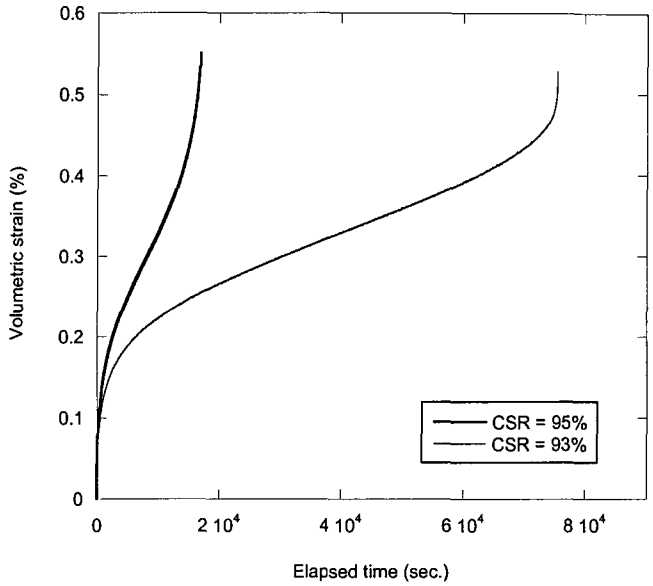

Figure 3.5 Elapsed time vs. volumetric strain at two different creep stress ratios CSR (i.e. 0.95 and 0.93) under a confining pressure σ_{11} of 40 MPa (Experimental results)

Furthermore, the elapse times to creep failure are given as a function of the creep stress ratio ranging from 0.9 to 0.98 by the closed triangles in Fig. 3.4 The experimental results fit the solid line well, which were obtained from the analyses using $n = 50$ and $A = 2.0 \times 10^{-23}$. The value of $n = 50$ is slightly larger than the values reported by Sano and Kudo (1992b), but is within the range reported by Atkinson (1984). It can be stated, on a qualitative basis at least, that the experimental results are in good accordance with those analyzed numerically under the conditions of $n = 50$ and $A = 2.0 \times 10^{-23}$.

3.6.2.2 Effect of moisture

It is well known that time-dependent behaviors of rocks are seriously affected by water more than time-independent behaviors (e.j., Lajtai et al., 1987). Meredith and Atkinson (1983) studied the effects of water on sub-critical microcrack growth in basic

rocks, and reported that the sub-critical microcrack growth under moist conditions is much higher than that under dry conditions. To investigate the effect of moisture on sub-critical microcrack growth of Inada granite, the results of creep tests on wet Inada granite are shown in Fig. 3.6. To fit these results to the numerical analyses, we accepted $n = 50$, which was the same as that for the dry Inada granite, and $A = 10^{-22}$, which was five times larger than that for dry Inada granite. It can be said that moisture has a large influence to the parameter A rather than the parameter n. In relation to this point, Atkinson and Meredith (1987) experimentally investigated the effect of water on sub-critical microcrack growth parameters of granitic rocks. Interestingly, they found that the increase of humidity does not have a significant influence on the sub-critical microcrack growth index n, but rather results in large increase in microcrack growth velocity.

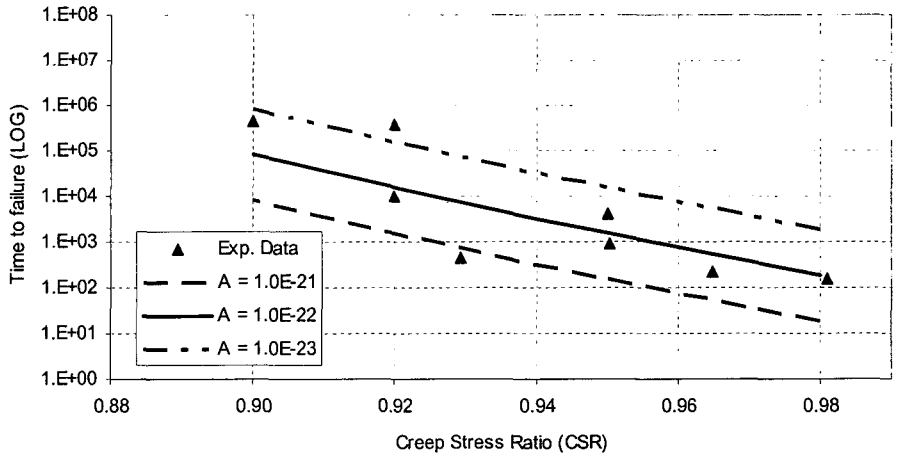

Figure 3.6 Creep stress ratio vs. time to failure at confining pressure of 40 MPa for Inada granite under wet conditions

3.7 LONG-TERM BEHVAIOR OF ROCK AROUND A CIRCULAR TUNNEL

A rectangular region ($500mm \times 500mm$) with a circular tunnel of 160 mm in diameter was analyzed by means of FEM in order to show the time-dependent development of the Excavation Disturbed Zone (EDZ). As shown in Fig. 3.7, the number of finite element meshes and nodes are 290 and 168 respectively, and the numbers 130, 232, 251 and 271 in Fig. 3.7 (b) show four locations of triangular meshes, in which growth of microcracks will be discussed later. All the parameters in the governing equations are selected as those for dry Inada granite (i.e., Table 1, $n = 50$ and $A = 2.0 \times 10^{-23}$). The rectangular region was subjected, on a tentative basis, to the far field stresses of $\sigma_{11} = 10$ MPa and $\sigma_{22} = 70$ MPa under a plan stress conditions.

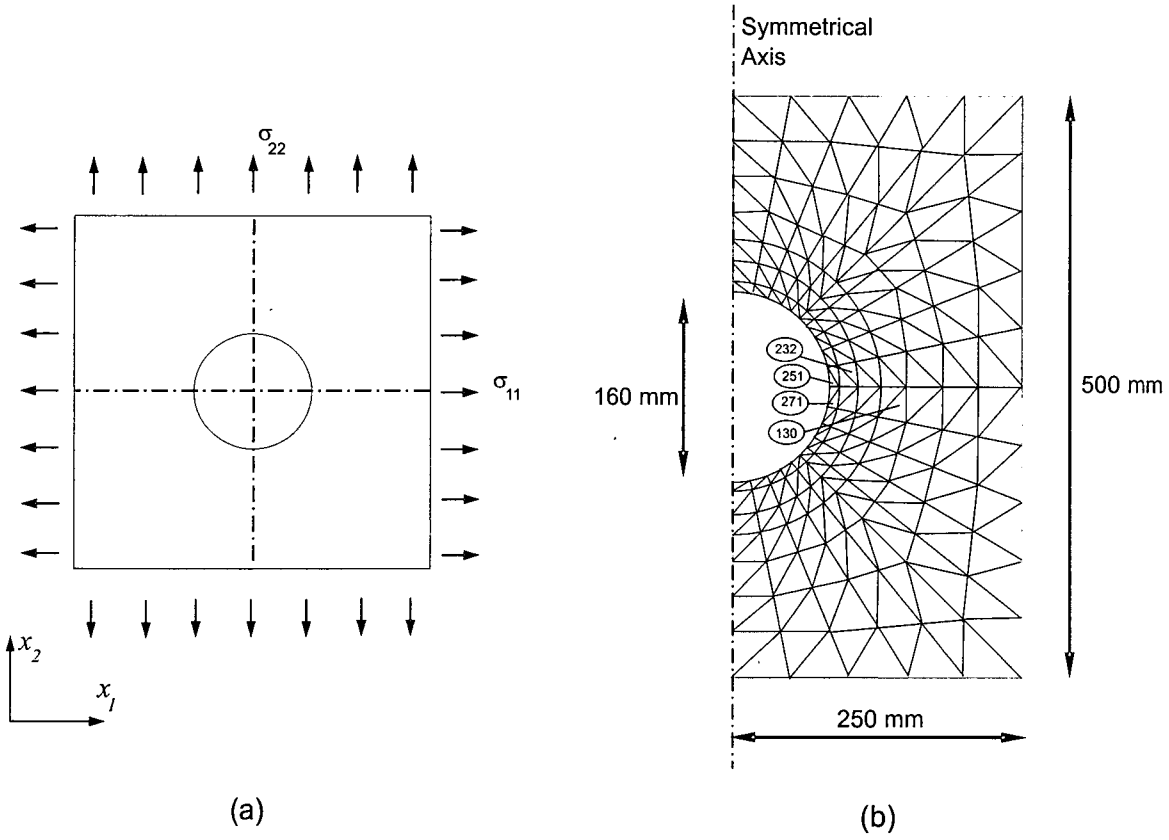

Figure 3.7 (a) Sample with a circular hole, (b) Finite element mesh

Figs 3.8 (a) to (h) show the time-dependent development of EDZ around the circular tunnel by illustrating microcrack length at eight different time steps. The following observations are worth noting:

1) Disturbed zones are mainly developed in the vicinity of the sidewalls of the tunnel in the case that the vertical stress σ_{22} is larger than the horizontal stress σ_{11}. Fakhimi et al. (2001) obtained the similar result in the analysis of stress-induced damage zones around a circular tunnel. Meglis et al. (2001) also reported the similar trend in a real tunnel by constructing a two-dimensional tomographic image of wave velocity.

2) Microcracks continue to grow all the time, particularly in the vicinity immediately adjacent to the tunnel wall, until failure finally takes place. Here, "failure" means that microcracks tend to grow without a limit so that no convergence is attained in the iterative calculation.

Figs 3.9 (a)-(c) illustrate the progressive change of microcrack length as a function of time in the four typical triangular meshes 130, 232, 251 and 271 (Fig. 3.7 (b)). The observations are done at three different elapse times; i.e. (a) 10 yrs, (b) 450 yrs, and (c) 550 yrs. If the calculation is stopped at 10 years, the two meshes (130 and 232) remain in the primary creep stage, while the two meshes (251 and 271) reach the secondary creep stage. If the calculation is continued until 550 years, the former meshes 130 and 232 still remain in the primary creep, while the later meshes 251 and 271 reach the tertiary creep so that microcracking becomes eventually unstable.

It should be quickly pointed out, however, that the results in Figs 3.8 and 3.9 are totally dependent on how accurately the material parameters are determined. In particular, the parameters controlling sub-critical crack growth are of great importance to get reliable results on the time-dependent growth of microcracks. In this study, these parameters were determined using creep tests, which lasted only for ten days. More experimental studies are needed to improve the predictive value of the model.

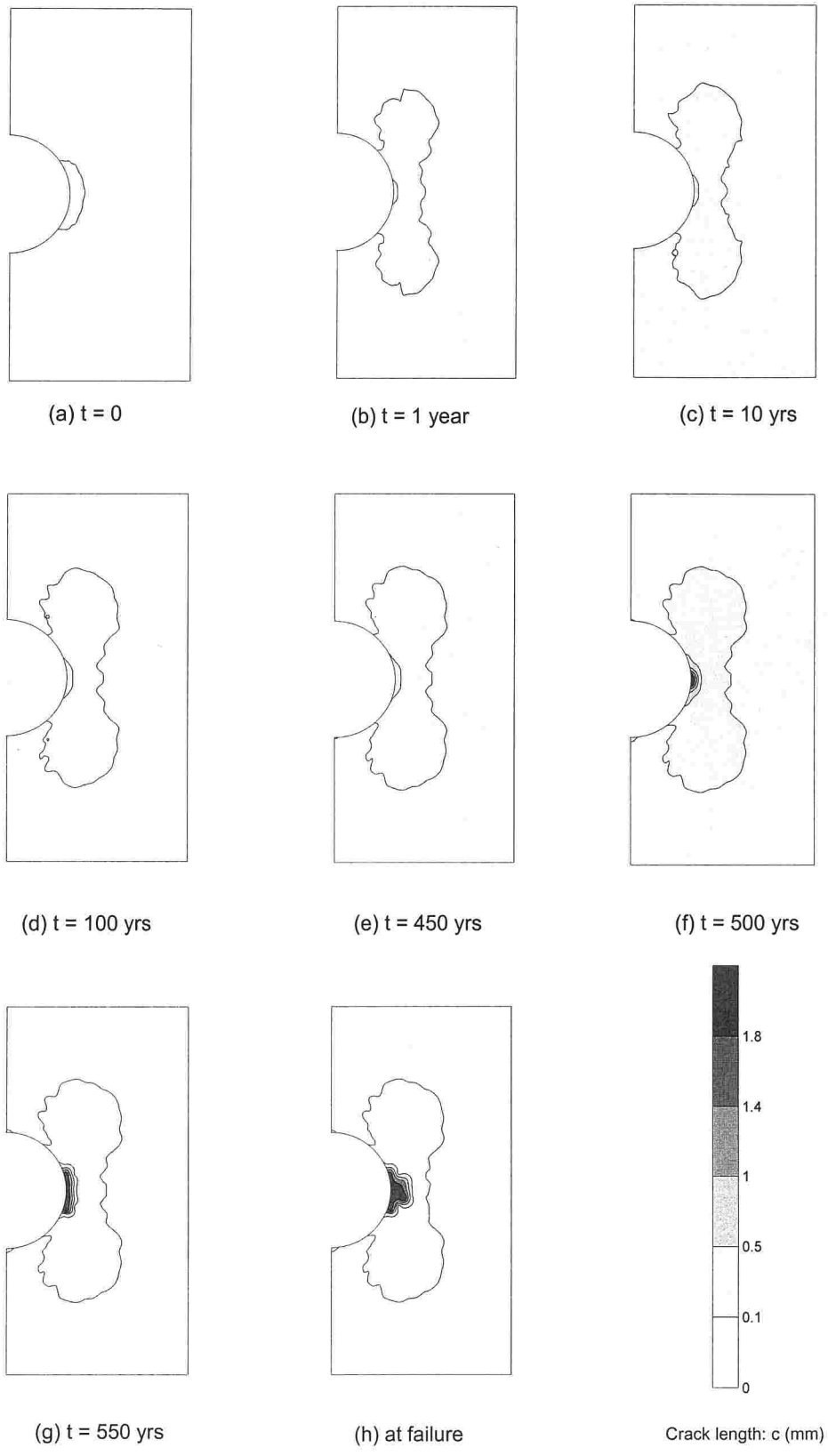

Figure 3.8(a)-(h). Time-dependent development of damage zone around the hole

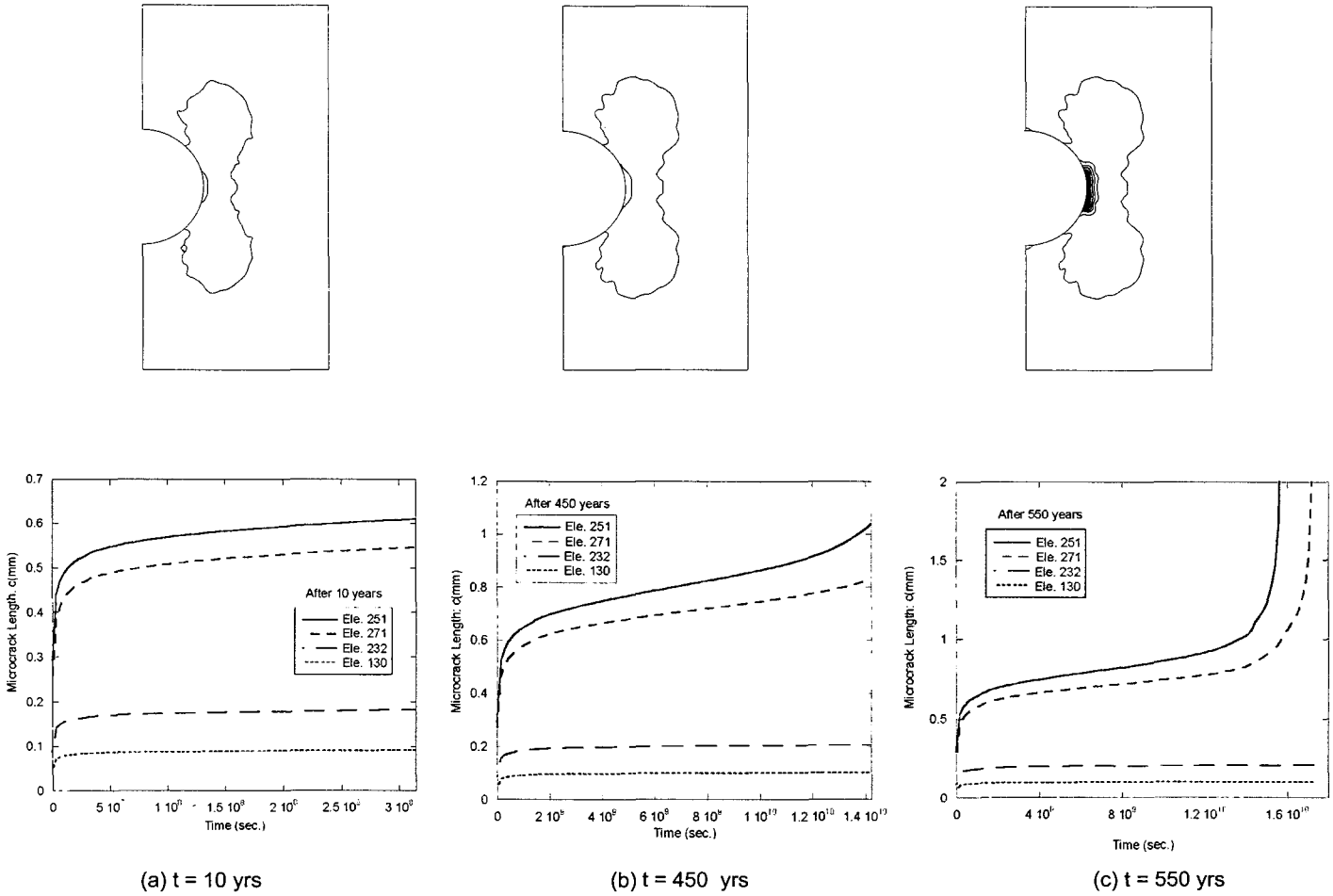

(a) t = 10 yrs (b) t = 450 yrs (c) t = 550 yrs

Figure 3.9 Microcrack length growth in four elements for (a) t = 10 yrs, (b) t = 450 yrs and (c) t = 550 yrs.

3.8 CONCLUSIONS

The micromechanics-based continuum damage model proposed by Golshani et al. (2006) was extended so that time-dependent behaviors of brittle material could be taken into account, with special interest in the numerical analysis of the Excavation Damage Zone (EDZ) around a tunnel. Using Inada granite, we carried out creep tests in a triaxial vessel under a confining pressure with the following two objectives; i.e. to see how the damage growth model can predict the time-dependent behaviors of brittle materials like Inada granite, and to determine the model parameters involved in the model. The conclusions are summarized, as follows:

The present model is capable of reproducing the three characteristic stages of creep behavior (i.e., primary, secondary, and tertiary creep) commonly observed in laboratory creep tests.

The sub-critical microcrack growth parameters (i.e. n and A) can be determined for Inada granite by fitting the numerical results of elapsed time to failure versus creep stress ratio CSR curve with the experimental data under both dry and wet conditions. The results agree with the fact that the presence of moisture reduces creep failure time. It is found that the moisture condition significantly influences the parameter A rather than the parameter n.

Use of the extended model makes it possible to analyze not only the extension of microcrack length, but also the development of the EDZ around tunnels as a function of time. The disturbed zones are mainly developed in the sidewalls of the tunnel in the case that the vertical stress σ_{22} is larger than the horizontal stress σ_{11}. Microcracks continue to grow continuously, particularly in the vicinity immediately adjacent to the tunnel walls, until failure takes place.

The present model underestimates the volumetric strains observed experimentally in creep tests of Inada granite. More refinement of the model is needed, in particular, in the kinematic model of crack opening.

REFERENCES

Adhikary, D. P. and Dyskin, A. V. (1997): Modelling the deformation of underground excavations in layered rock masses, *Int. J. Rock Mech. Min. Sci.,* 34, pp. 714-719.

Atkinson, B. K. (1980): Stress corrosion and the rate-dependent tensile failure of a fine-grained quartz rock, *Tectonophysics*, 65, 281.

Atkinson, B. K. (1984): Sub-critical crack growth in geological materials, *J. Geophys. Res.*, 89, pp. 4077-4114.

Atkinson, B.K. and Meredith, P.G. (1987): The theory of sub-critical crack growth with applications to mineral and rocks In: Fracture mechanics of rock, London: Academic press, pp.110-166.

Chen, W. Z., Zhu, W. S. and Shao, J.F. (2004): Damage coupled time-dependent model of a jointed rock mass and application to large underground cavern excavation, *Int. J. Rock Mech. Min. Sci.,* 41, pp. 669-677

Costin L. S. and Mecholsky (1983): Time-dependent crack growth and failure in brittle rock, P*roc. 24th U.S. Symposium on Rock Mechanics*, Texas A&M Univ., College station, TX, June 20-23, 1983.

Fakhimi, A., carvalho, F., Ishida and T., Labuz, J. F. (2002): Simulation of failure around a circular opening in rock, *Int. J. Rock Mech. Min. Sci.,* 39, pp. 507-515

Golshani, A., Okui, Yoshiaki, Oda, Masanobu and Takemura, Takato (2006): A micromechanical model for brittle failure of rock and its relation to crack growth observed in triaxial comopression tests of granite, *Mechanics of Materials*, 38(4), pp288-203.

Hallbauer, D.K., Wagner, H. and Cook, N. G.. W. (1973): Some observations concerning

the microscopic and mechanical behavior of quartzite specimens in stiff, triaxial compression test, *Int. J. Rock Mech. Min. Sci. & Geomech. Abstr.*, 6, pp. 713-726.

Hommand-Etienne, F., Hoxha, D. and Shao, J.F. (1998): A continuum damage constitutive law for brittle rocks, *Computer and Geotechnics*, 22 (2), pp. 135-151.

Horii, H. and Nemat-Nasser S. (1985a): Compression-induced microcrack growth in brittle solids: axial splitting and shear failure, *Journal of Geophysical Research*, 90, pp. 3105-3125.

Horii, H. and Nemat-Nasser S. (1985b): Elastic fields of interacting inhomogeneities, *Int. J. Solids Struct.*, 21, pp. 731-745.

Horii, H. and Nemat-Nasser, S. (1986): Brittle failure in compression: splitting, faulting and brittle-ductile transition, *Phil. Trans. R. Soc. Lond.*, A 319, pp. 337-374.

Hou, Z. (2003): Mechanical and hydraulical behavior of rock salt in the excavation disturbed zone around underground facilities, *Int. J. Rock Mech. Min. Sci.*, 40, pp. 725-738.

Kranz, R. L. (1979): Crack growth and development during creep of Barre granite, *Int. J. Rock Mech. Min. Sci. Geomech. Abstr.*, 16, pp. 23-35.

Lajtai, E. Z., Schmidtke, R. k. and Bielus, L. P. (1987): The effect of water on the time-dependent deformation and fracture of a granite, *Int. J. Rock Mech. Min. Sci. Geomech. Abstr.*, 24, pp. 247-255.

Martin, R. J. (1972): Time-dependent crack growth in quartz and its applications to the creep of rocks, *J. Geophys. Res.*, 77, 1406.

Martino, J. B. and Chandler, N. A. (2004): Excavation-induced damage studies at the underground research laboratory, *Int. J. Rock Mech. Min. Sci.*, 41, pp. 1413-1426.

Meglis, L. L., Chow, T. and Young, R. P. (2001): Assessing microcrack damage around a tunnel at the underground research laboratory using ultrasonic velocity tomography, 38th Rock Mechanics Symposium, DC Rocks, Washington D.C., U.S.A., July 7-10, pp. 919-925.

Meredith, P.G. and Atkinson, B.K. (1983): Stress corrosion and acoustic emission during tensile crack propagation in Whin Sill Dolerite and other basic rocks, *Geophys. J. Astr.*, 75, pp. 1-21.

Mitami, S, and Detournay, E. (2004): Damage around a cylindrical opening in a brittle rock mass, *Int. J. Rock Mech. Min. Sci.,* 41, pp. 1447-1457.

Nemat-Nasser, S. and Obata, M. (1988): A microcrack model of dilatancy in brittle materials, *Journal of Applied Mechanics*, Vol. 55, pp. 24-35.

Nemat-Nasser, S. and Hori, M. (1993): Micromechanics: overall properties of heterogeneous materials, North-Holland, Netherlands, p.687.

Oda, M., Katsube, T. and Takemura, T. (2002): Microcrack evolution and brittle failure of Inada granite in triaxial compression tests at 140 MPa, *Journal of Geophysical Research*, Vol. 107, NO. B10.

Okui, Y., Horii, H. and Akiyama, N. (1993): A continuum theory for solids containing microdefects, *Int. J. Eng. Mech.*, Vol. 31, No. 5, pp. 735-749.

Potyondy, D.O., Cundall, P.A. (1998): Modeling-formation mechanisms in the URL mine-by test tunnel using bonded assemblies of circular particles, *Int. J. Rock Mech. Min. Sci.,* 35, No. 4/5, paper No. 067.

Read, R.S. (2004): 20 years of excavation response studies at AECL's Underground Research Laboratory, *Int. J. Rock Mech. Min. Sci.,* 41, pp. 1251-1275.

Sano, O., Kudo, Y. and Mizuta, Y. (1992a): Experimental determination of elastic constants of Oshima granite, Barre granite, and Chelmsford granite, *Journal of Geophysical Research*, Vol. 97, NO. B3, pp. 3367-3379.

Sano, O. and Kudo, Y. (1992b): Relation of fracture resistance to fabric for granitic rocks, PAGEOPH, Vol. 138, No.4, pp. 656-677.

Scholtz, C. H. (1968): Microfracturing and the inelastic deformation of rock in compression, *Journal of Geophysical Research*, 73, No.4, pp. 1417-1432.

Souley, M., Homand, F., Pepa, S. and Hoxha, D.(2001): Damage-induced permeability changes in granite: a case example at the URL in Canada, *Int. J. Rock Mech. Min. Sci.*, 38, pp. 297-310.

Takemura, T., Golshani, A., Oda, M. and Suzuki, K. (2003): Preferred orientation of open microcracks in granite and their relation with anisotropic elasticity, *Int. J. Rock Mech. Min. Sci.*, 40, pp. 443-454.

Waversik, W. R. and Brace, W. F. (1979): Post-failure behavior of granite and diabase, *Rock Mech.*, 3, pp. 61-85.

Wong, T. F. (1982): Micromechanics of faulting in Westerly granite, *Int. J. Rock Mech. Min. Sci. & Geomech. Abstr.*, Vol. 19, pp. 49-64.

Wong, R. H. C., Lin, P., Tang, C.A. and Chau, K.T. (2002): Creeping damage around an opening in rock-like material containing non-persistent joints, *Engineering Fracture Mechanics*, 69, pp. 2015-2027.

Chapter 4

Conclusions and Future Studies

4.1 CONCLUSIONS

A Micromechanics-based continuum damage model for brittle failure of rock under compression has been proposed to provide a numerical tool for analyzing not only the macro-scale mechanical responses of rock such as strength, but also the microscopic events which take place in association with the inelastic deformation in rock. Special emphasis is placed on how to predict numerically the changes in crack length and crack density during inelastic deformation ending up with brittle failure. If this can be done successfully, the numerical code based on the micromechanics-based continuum damage model can easily be extended to analyze coupling behavior between microcrack growth and the fluid flow through rock. The pre-existing cracks may be randomly distributed or may have an initial preferential distribution. They may be of varying sizes and orientations. The effects of interaction among microcracks are directly taken into account in the constitutive equations (cracks are dealt with together). For considering the interaction effects, the generalized form of Interaction Filed Theory IFT for microcracks with different orientation, was used. A small number of parameters are involved in this model and each one is physically meaningful and can be identified from standard laboratory tests.

In chapter 2, the proposed model for brittle failure of rock under compression was

explained. First a microcrack growth model for a single microcrack was proposed. This model is based on tensile crack mechanism and crack propagates along its surface. Then, the effect of interaction among microcracks which evaluated directly using the generalized form of Interaction Filed Theory IFT was discussed. The constitutive equation for elastic materials containing many microcracks with different orientations was proposed next and finally, determination of model parameter was explained. Note that, in this model, stress-strain relationship at any point depends on the stress and crack geometry at all points in the body. In other words, since the behavior of material depends on the stress and crack geometry at other points, the derived constitutive equation is understood as non-local. Also, comparisons between the model's predictions and experimental result have been made in this chapter. In contrast to other numerical models we have information not only on the mechanical response of rocks but also on cracks geometry evolution. Although some simplifications are assumed in the formulation, the proposed model agrees well with experimental data. The predicted strength for Inada granite of the proposed model is in good agreement with experimental data. However for uniaxial compression test, the numerical result is overestimated due to different mechanism of fracture. In spite of the gap between numerical and experimental results for cracks growth and denisty, one can notice that there is a qualitatively good prediction by this model and cracks growth is correctly described. This gap is caused by some simplifications such as assumption of constant cracks density which is made in the numerical simulation.

In chapter 3 the proposed model was extended so that time-dependent behaviors of brittle material could be taken into account, with special interest in the numerical analysis of the Excavation Damage Zone (EDZ) around a tunnel. Using Inada granite, we carried out creep tests in a triaxial vessel under a confining pressure with the following two objectives; i.e. to see how the damage growth model can predict the time-dependent behaviors of brittle materials like Inada granite, and to determine the model parameters involved in the model. The sub-critical microcrack growth parameters (i.e. n and A) can be determined for Inada granite by fitting the numerical results of elapsed time to failure versus creep stress ratio CSR curve with the experimental data under both dry and wet conditions. The results agree with the fact that the presence of

moisture reduces creep failure time. It is found that the moisture condition significantly influences the parameter A rather than the parameter n. Use of the extended model makes it possible to analyze not only the extension of microcrack length, but also the development of the EDZ around tunnels as a function of time. The disturbed zones are mainly developed in the sidewalls of the tunnel in the case that the vertical stress σ_{22} is larger than the horizontal stress σ_{11}. Microcracks continue to grow continuously, particularly in the vicinity immediately adjacent to the tunnel walls, until failure takes place.

4.2 FUTURE STUDIES

On the contrary to constant cracks density assumption, in fact, the cracks density varies during loading process; some neighboring microcracks join each other and make larger cracks. Close to failure, the cracks coalescence especially gives rise to the appearance of longer cracks which leads to failures (Hoxha and Homand, 2000). Also, new microcracks called stress-induced cracks (Oda et al., 2002a) may nucleate. The three-dimensional (3D) cracks density changes with differential stress increasing have been shown in chapter 2 (Figure 2.24) for Inada granite. The cracks density decreases while Inada granite is loaded up to 90% of failure stress and remains almost constant beyond that up to failure occurs. An extension of the present study is to assume cracks density varies for instance, function of axial loading. For this purpose, some experiments must be carried out in different stages of axial loading.

In this model, it is assumed that the matrix material remains elastic during loading and that all inelastic deformation is due to microcracking and in calculation of the inelastic strain, we only considered inelastic strain due to changes in microcrack displacement caused by applied loads. Including the inelastic deformation due to microcrack opening and slip can be considered as another extension of this study.

Published papers

- "A micromechanical model for brittle failure of rock and its relation to crack growth observed in trixial compression tests of granite", Mechanics of Materials, 38, 2006, pp. 287-303.

- "Hydraulic behaviour of Inada granite in the excavation disturbed zone around underground openings", The Seventh International Summer Symposium, JSCE, 30 July 2005 Tokyo, Japan, pp. 153-156.

- "Simulation of damage around a circular opening in rock". The 11th International Conference of IACMAG, 19-24 June, 2005, Turin, Italy, pp. 33-40.

- "Time-dependent continuous damage model for brittle failure of rocks", 53rd Geomechanics Colloquy and EUROCK 2004, 7-9 October, 2004, Salzburg, Austria, pp.701-706.